Small strain stiffness, microstructure and other characteristics of an allophanic volcanic ash

GOBIN, Mukteshwar
Department of Civil Engineering, Kyushu University

YASUFUKU, Noriyuki
Department of Civil Engineering, Kyushu University

LIU, Guojun
Changshu Institute of Technology

WATANABE, Midori
Center of Advanced Instrumental Analysis, Kyushu University

他

出版情報：Engineering Geology. 313, pp.106967-, 2023-02. Elsevier
バージョン：
権利関係：

Small strain stiffness, microstructure and other characteristics of an allophanic volcanic ash

M. Gobin[1,*], N. Yasufuku[2], G. Liu[3], M. Watanabe[4], R. Ishikura[5]

[1] M. Gobin, Ph.D. Student, Department of Civil Engineering, West Building 2, Room 1108-1, Kyushu University, 〒 819-0395 Motooka 744, Nishi-ku, Fukuoka, Japan (*corresponding author). E-mail: gobin.mukteshwar.918@s.kyushu-u.ac.jp; muktesh01@ yahoo.co.uk

[2] N. Yasufuku, Professor, Department of Civil Engineering, Kyushu University, 〒 819-0395 Motooka 744, Nishi-ku, Fukuoka, Japan. E-mail: yasufuku@civil.kyushu-u.ac.jp

[3] G. Liu, Lecturer, Ph.D., Changshu Institute of Technology, 215500, Changshu, Suzhou, Jiangsu Province, People's Republic of China. E-mail: guojun.liu@cslg.edu.cn

[4] M. Watanabe, Assistant Professor, Center of Advanced Instrumental Analysis, Kyushu University, 〒 819-0395 Motooka 744, Nishi-ku, Fukuoka, Japan. E-mail: watanabe.midori.452@m.kyushu-u.ac.jp

[5] R. Ishikura, Associate Professor, Department of Civil Engineering, Kyushu University, 〒 819-0395 Motooka 744, Nishi-ku, Fukuoka, Japan. E-mail: ishikura@civil.kyushu-u.ac.jp

Abstract

Small strain mechanical properties are a prerequisite for seismic analysis and design. Corresponding studies on volcanic soils are by themselves limited while research on some volcanic ashes which intrinsically have high fines content is even rarer. Presence of clay minerals like allophane and imogolite confers uncharacteristic properties to the soils which somehow seems underappreciated. This is evidenced, for instance, by the near absence of literature related to the 2016 Kumamoto Earthquake explicitly mentioning the influence of these particular clay minerals. Against this background, this study aimed at partially filling the gap with respect to the small strain shear modulus, G_{max} of an allophanic volcanic ash and underline the influence of allophane and imogolite on some of the soil properties. Remoulded black volcanic ash, kuroboku was sampled from two sites in the Kyushu area in the south of Japan. As part of the experimental work, a series of index properties, engineering properties, electron microscope (Scanning Electron Microscope (SEM) and Field Emission Scanning Electron Microscope (FE-SEM)) examinations and bender element (BE) tests was performed on these soils. The paper elaborates on the peculiar characteristics of the allophanic volcanic ash, including presence and effect of water of crystallization and influence of electrostatic bonding on grain size distribution and liquefaction resistance. Based on the SEM and FE-SEM images, the microstructure of the kuroboku soils was assessed in terms of its various components, the contact relation and the pore space. Observations from the microscopy analysis like presence of diatoms and intra-elemental pores were key to understanding the slight variation in the G_{max} among the tested soils. An attempt was also made at situating the G_{max} of the kuroboku soil vis à vis other types of soils. Empirical relationships for estimating the G_{max} of kuroboku separately and with other volcanic soils were proposed. Findings from this research could rekindle an interest into further understanding the particular characteristics of allophanic materials as well as encourage more research on their dynamic properties, which is essential considering that these materials are mostly found in seismically active regions.

Keywords: Allophanic volcanic ash, microstructure, bender element, grain size distribution, liquefaction, shear modulus

1. Introduction

The proper estimation of dynamic properties of soils ensures that inter alia, realistic analysis of seismic response and ground deformation as well as liquefaction evaluation may be made. One such property is the shear stiffness which shows a general non-linear variation. Nonetheless, at strain levels less than 0.001%, the shear stiffness is considered to be constant and termed as the small strain shear modulus, G_{max} (Gu *et al.*, 2015).

The small strain shear modulus has been commonly estimated by seismic tests in the field or by resonant columns (RC) and torsional stiffness (TS) device in laboratory. Lawrence (1963) and Shirley and Hampton (1978) carried out pioneering work on the application of piezo-ceramic transducers (more commonly known as bender element (BE)) for estimating the shear wave velocity. Since then owing probably to its lower cost and versatility in being incorporated into different experimental devices, the BE has become a popular method for estimating the shear velocity, V_s from which G_{max} may then be evaluated (Viggiani & Atkinson, 1995; Ferreira *et al.*, 2007; Yamashita *et al.*, 2009; Clayton, 2011; Le *et al.*, 2014; Dao *et al.*, 2015; Choo *et al.*, 2015; Ying *et al.*, 2021; Pan *et al.*, 2022).

The current state of the art on the small strain shear modulus is essentially based on sedimentary and clayey soils. Efforts have been made in recent years to fill the gap with respect to the small strain stiffness of some unconventional soils like calcareous sands and loess (Giang *et al.*, 2017; Song *et al.*, 2017; Liu *et al.*, 2019). At the same time, many researchers have highlighted that the small strain mechanical behaviour of volcanic soils (one of the tricky soils in geotechnical engineering) is less extensively studied compared to sandy soils (Sahaphol & Miura, 2005; Senetakis *et al.*, 2012; Liu *et al.*, 2016). Furthermore, it is noteworthy to add that this "limited" existing literature is on volcanic soils with low fines content. Orense *et al.* (2006) used cyclic tests to determine the G_{max} of volcanic soil from Mount Pinatubo in Philippines which had less than 5% fines content. Liu *et al.* (2016), reported a figure of 7% for fines content of the volcanic soils obtained from the Naganuma area in Japan. Okewale and Grobler (2020) studied the G_{max} of completely decomposed volcanic rocks from Hong Kong, with the original soil sample having less than 20% fines. In the same vein Asadi *et al*. (2020) investigated the shear modulus of pumiceous sand from New Zealand with fines content varying between 2.5% to 16.7%.

Research on the small strain shear modulus of volcanic ashes, which by their very nature have high fines content, is even scantier. On a global scale, Leamy (1984), Takahashi and Shoji (2002) and Fiantis *et al.* (2019) stated that volcanic ash soils cover approximately 0.84% of the land surface. On a regional scale, Hernandez *et al.* (2018) mentioned that volcanic ash soils can cover a much larger area for countries located

on the Andean mountains. For instance Rendón *et al.* (2020) mentioned that in Colombia, volcanic ash cover about 11.6% of the country while Martínez *et al.* (2021) reported a figure of 30% for Ecuador. Lowe and Palmer (2005) stated that andisols of the "allophanic" type cover about 12.5% of the New Zealand territory.

In Japan around 31% of the land surface is covered by andosols (National Agriculture and Food Research Organization (NARO), 2022). The Kyushu area in the south of Japan is home to many active volcanoes and is largely covered by andosols like black allophanic volcanic ash, which is locally known as kuroboku - kuro and boku meaning black and soil respectively in Japanese (Kitazono, 1987; Tamura *et al.*, 2021). In the subsequent part of this document, the black volcanic ash will be denoted as kuroboku. Kitazono (1985) and Komine (2007) as cited in Yasuhara *et al.* (2012) mentioned that due to their abundance, these andosols are used as geomaterials like in the construction of levees and embankments.

Following the 2016 Kumamoto earthquake which rattled the Kyushu Island, significant damage was caused to natural deposits and earth structures, with the cost initially estimated to be around 2.4 to 4.6 trillion yen (Cabinet Office of Government of Japan, 2016). Mukunoki *et al.* (2016) suggested that the geological features of the area and the characteristics of the volcanic ash as possible factors for making the area ripe to geo-disasters. The landslides which occurred near the Aso bridge (Aso-Ohashi in Japanese) and Takanodai attracted the attention of many researchers and allowed the Soil Engineering Community to surmise the possible failure mechanisms tied to these events.

Chiaro *et al.* (2018a) mentioned the difficulty in obtaining G_{max} data of the kuroboku soil for the purpose of modelling the Takanodai landslide and instead using G_{max} of volcanic ash found in New Zealand. Moreover, from an "Advanced search" on Google Scholar from 2016 to June 2022, with respect to the Kumamoto earthquake, it was also surprising to find that no Soil Engineering publications referred to the clay mineral imogolite. Furthermore, only a handful of peer-reviewed publications made reference to allophane, without explicitly explaining how the very presence of this material influences the behaviour of the soil.

It seems reasonable to say that allophane and imogolite still lack appreciation in the Soil Engineering Community, since we cannot dissociate the properties of the soil from the characteristics of these clay minerals. Indeed, quoting Vaughan (1985), Wesley (2010) emphasized that some of the properties of allophanic soils do not universally align with those of sedimentary materials. Against this backdrop and considering the recurrence of seismic and volcanic activities in the area, it seems warranted to partially fill the gap in literature with respect to the small strain stiffness of this particular type of soil, and at the same time shed more light on the characteristics of allophane and imogolite.

This paper aims at addressing the above two points. At first, a brief overview of the clay minerals allophane and imogolite is provided, followed by information about the geological and climatic conditions of the two sites in central Kyushu from which remoulded kuroboku soil was sampled. The paper then presents a detailed discussion about the microstructure of the kuroboku soil, as well as highlighting features proper to these allophanic soils like their flocculating nature and electrostatic bonding and how these influence the liquefaction resistance and engineering properties. The results of the small strain shear stiffness obtained from an extensive set of BE tests, carried out over a wide range of void ratios and effective confining stresses are discussed. Empirical relationships for estimating the shear modulus of the kuroboku soils were proposed. Finally an attempt was made at situating the G_{max} data obtained in this study vis à vis other soils in the literature.

2. Overview of allophane and imogolite

Allophane and imogolite are two clay minerals formed from the weathering of volcanic ash material (Eswaran, 1972). Fieldes (1955) initially postulated that volcanic glass would first weather to allophane followed by halloysite and kaolinite. From the comprehensive review of Harsh *et al.* (2002) and Moon *et al.* (2015) of the works of several researchers since the 1980s, we can come to terms with the alternative viewpoint in that it is the concentration of Si in the soil, availability of Al and drainage conditions that determines the formation of either allophane or halloysite. Nonetheless, this divergent hypothesis still seems not well popularized considering that Chen and Lee (2004), Herrera *et al.* (2007), Verdugo (2008), Wesley (2010), Hernandez *et al.* (2018) and Menendez *et al.* (2022) referred only to the weathering sequence proposed by Fieldes.

In brief, allophanes are short range order hydrous aluminosilicates, which depict a fibrous and globular morphology (Wells & Theng, 1985; Wada, 1989). Henmi and Wada (1976) reported that allophanes are hollow spherules with an outside diameter of about 3.5 to 5nm. These individual hollow spherules in turn may aggregate together to form a domain (Rao, 1995).

Imogolites, on the other hand, are long range paracrystalline aluminosilicates and occur together with allophanes (Wada, 1978; Verdugo, 2008). It is worthwhile to mention that the presence of imogolite was first confirmed by Yoshinaga and Aomine in 1962 from samples taken in Hitoyoshi, Kumamoto, which is only a few kilometres away from the sampling sites in this research. Wada *et al.* (1970) mentioned that imogolites are filiform units having an outside diameter between 1.7 and 2.1 nm and length extending up to several micro metres.

Allophanic soils are present in all continents across the world. Pacific rim countries like Japan, Indonesia, Papua New Guinea, Hawaii, New Zealand as well as South American countries like Chile, Ecuador and Colombia are known to be abundantly covered with this type of soil. Carribean Islands (like Domina), South Korea (Jeju Island), Italy, Iceland, North Western United States of America, Australia, Antarctica and some African countries with soils of volcanic origins like Cameroon, Nigeria and Reunion Island have also been reported as having allophanic soils (Sieffermann & Millot, 1969; Wada *et al.*, 1972; Wallace, 1973; Maeda *et al.*, 1977; Ola, 1980; Webb & Finlayson, 1984; Goldsmith & Smith, 1985; Rouse, 1990; Reading, 1991; Ugolini *et al.*, 1991; Wada *et al.*, 1992; Song & Yoo, 1994; Rao, 1996; Fiorillo & Wilson, 2004; Frattini *et al.*, 2004; Simas *et al.*, 2006; Herrera *et al.*, 2007; Verdugo, 2008; Levard, 2012; Rocchi *et al.*, 2017; Martínez *et al.*, 2021). Moreover, the presence of the allophane mineral has also been confirmed on planet Mars (Bishop & Rampe, 2016).

3. Geology, Test material and Methodology

3.1 Geological setting

The Kyushu Island lies above the Benioff zone created by the subduction of the Philippine Sea Plate, west south west of the Nankai Trough (Figure 1a). The studied sites are located in a seismically active area, with several known active fault system and many active volcanoes like Mount Aso and Mount Kuju (Figure 1b). The sites are bounded to the north by the Beppu-Shimabara volcanic graben and to the south by a shear zone - Median Tectonic Line (MTL). Ikeda *et al.* (2009) stated that the MTL is one of the longest active strike-slip faults in Japan, with the stress conditions being of transtention nature in Kyushu and western part of Shikoku islands. The stress conditions changes to transpression type on the eastern part of Shikoku and onto Honshu islands.

Matsuda (1981) had mentioned that nearly 80% of the destructive earthquakes in Japan between 1885 and 1979 happened along or near active faults. High magnitude earthquakes were forecasted along or close to active fault lines greater than 10 km. Following the same pattern, in the 2016 Kumamoto Earthquake, the foreshock event on 14 April occurred at a depth of 11.39 km on the Hinagu fault, while the mainshock event of 16 April event occurred at a depth of 12.45 km on the Futagawa fault (Shirahama *et al.*, 2016). Both Hinagu and Futagawa were long recognized fault lines (Doi *et al.*, 2019). After the Kumamoto Earthquake, Suzuki (2017) and the Geospatial Information Authority of Japan (2022a; 2022b) confirmed the presence of other active fault lines and mapped the numerous surface ruptures observed. These surface ruptures and "new" or "reactivated" fault lines around Site 2 were plotted in Figure 1c. A photo of surface ruptures in

Kawayo village captured on 18 April 2016 is shown in Figure 1d - View A. The following elements can be highlighted:
(i) the Futagawa fault was confirmed to have extended in the east north east direction; (ii) the presence of an active fault under the Kurokawa river at the foot of Site 2 was also recognized; (iii) numerous surface ruptures were confirmed especially in Kawayo, Minami Aso as well as some "new" or "reactivated" active faults, although their precise positions were unclear.

3.2 Test material

Remoulded kuroboku soil was collected from two forested sites in central Kyushu. Soil 1 (from Site 1) was sampled in Naoiri in Oita prefecture, while Soil 2 (from Site 2) was gathered from a plot just adjacent to the Aso-Bridge landslide site in Kumamoto prefecture. The soils were sampled from a depth of about 1.5m. Both soils are dark andosols, with the colour of Soil 1 being 10YR2/1 (Figure 2(a)) and that of Soil 2 being 10YR3/2 (Figure 2(b)) according to the Munsell notation (YR is short for Yellow Red and represents the hue).

The parent rocks at Site 1 are welded pyroxene andesite from the Imachi pyroclastic flows (Figure 3(a)), just off the Serikawa pyroclastic flow geological series. The Imachi pyroclastic flows emanated from the second eruption cycle (850±30ka) of the now buried Shishimuta caldera (Takashima *et al.*, 2017). Site 2 lies on the western rim of Mount Aso, the largest caldera in Japan with a size of about 25 km and 18 km in the north south and east west direction respectively. As can be observed from the geological map around Site 2 in Figure 3(b), a notable characteristic of Mt. Aso is the variation of rock types (basalt, rhyolite, andesite and dacite) within a single volcanic group. The parent rock at Site 2 is pyroxene andesite (Aso Volcano products of pre-caldera stage). According to Nakada *et al.* (2016), there have been four major eruptions of Aso volcano since the Middle Paleolithic period. These are commonly referred as Aso-1 (270ka), Aso-2 (140 ka), Aso-3 (120ka) and Aso-4 (90ka).

The locations from which the soils were sampled have a temperate climate. The average annual rainfall at both sites is in excess of 2000mm (Japan Meteorological Agency, 2022a & 2022b). Thus, in accordance with the simplified allophane-halloysite rainfall (Si) leaching model mentioned by Mc. Daniel *et al.*, 2012, allophane formation would be favoured over halloysite at the sampling areas.

3.3 Sample preparation

Along with the natural soils 1 and 2, five other soils were prepared from the parent material. Soils 1A, 1B and 1C were sieved from Soil 1 and soils 2A and 2B were sieved from Soil 2. Soil 1A was prepared by wet sieving through 75µm sieve, soil 1B was the material that passed through 38µm sieve while soil 1C was the material retained on 38µm sieve. Soil 2A was obtained by wet sieving through 75µm sieve and soil 2B was obtained by sieving air dried Soil 2 through 425µm sieve.

For the wet sieving, the natural soils were first washed with a little water in an 850µm sieve to remove small rocks or other extraneous materials. The material passing the 850µm sieve was collected and washed through the other respective sieves (38µm and 75µm). The washed material from the 38µm and 75µm sieves were then left to settle before decantation. The decanted soils were finally stored in plastic containers to be ready for testing, as required.

3.4 Moisture content determination

The moisture content is conventionally determined by drying the soil to a constant mass at a temperature between 105° and 110°C. This method is based on the amount of "free water" loss by dying. But the drying temperature of 105-110°C may be too high for certain soils (Head, 1992). Observations by Terzaghi (1958) and Wesley (1973) assert the significant influence of temperature on moisture content determination for soils with allophane or halloysite minerals. Yasuda *et al.* (1999) may also be quoted as using a lower temperature of 60°C when assessing the wetting and drying behaviour of Kanto Loam (allophanic volcanic ash). The reasons as Fourie *et al.* (2012) highlighted is that some residual soils in addition to "free water", have "water of crystallization" that reside within the soil minerals.

To investigate whether the tested kuroboku had "water of crystallization", simultaneous tests were carried out on samples at 110°C and lower temperatures (50°C - 100°C). According to Fourie *et al.* (2012) a significant difference (> 6%) is said to indicate that "water of crystallization" is present and Schnaid and Huat (2013) recommend excluding it from moisture calculation. It was found that for kuroboku, the "water of crystallization" at 50°C was about 20%. For Soil 1, the average value stood at about 20.68% and for Soil 2 the value was about 19.58%. Figure 4 shows how the difference in water content varied with temperature. Therefore, in this study, the moisture content determination was adjusted for "water of crystallization" content. The adjusted natural water content for soils 1 and 2 were 160 and 157% respectively. Moreover, it should be highlighted that soils that were initially dried at 110°C and then soaked for 24 hours before being dried again at 50°C demonstrated that the "water of crystallization" had been irreversibly removed. In this particular case, the percentage difference in water content was less than 1%.

3.5 Index properties and grain size distribution

The liquid limit, LL and plastic limit, PL for soils 1 and 2 were determined according to JGS 0141. The plasticity chart for Soil 1 and Soil 2 is shown in Figure 5(a). Following air-drying, LL and PL stayed constant until the water content dropped to around 85% and 95% for soils 1 and 2 respectively. Beyond this water content threshold, the LL decreases more sharply than the PL (Figure 5(b)). Based on JGS 0051 – 2009, the volcanic ash soil used in this research could be categorised as volcanic cohesive soil (type II) - VH_2. The basic properties of the soils are summarized in Table 1 and Table 2.

To determine the grain size distribution, the laser diffraction particle size analyser SALD-3103, developed by Shimadzu Company was used. In this method, the soil particles are exposed to laser light. The intensity distribution pattern of the resulting diffracted and scattered light is then detected and analysed to find the size of the particles and their corresponding percentage composition. Hydrometer analysis was also carried out on soils 1 and 2. The grain-size distribution of the soils is shown in Figure 9.

3.6 Tri-axial test procedures

The triaxial samples, 50 mm in diameter and 100 mm in height, were prepared in five layers by using the moist tamping method. Moist tamping method has been used by several researchers to prepare volcanic ash samples. In fact Ishihara (1996) stated that with this method generally uniform specimens with less segregation can be produced for a wide range of void ratios. Verdugo (2008) used moist tamping to prepare remoulded samples of allophanic volcanic ash in Chile, while Chitravel *et al.* (2022) and Asadi *et al.* (2020) employed it to prepare samples of pumiceous volcanic ash from Japan and New Zealand respectively. Ferrari *et al.* (2013) resorted to this method for volcanic ash from Costa Rica. They mentioned that the moist-tamping technique used to prepare the specimens resulted in a soil fabric similar to that of the natural material. Tsukamoto *et al.* (2009) also used moist tamping on sandy volcanic ash soil, Shirasu. The soil at each layer was compacted by gentle tamping until the required thickness of each layer was achieved. It should be noted that for the preparation of very loose specimens, no significant tamping was used. The diameter of the specimen was then measured using a PI tape (the diameter used for computation is the average of at least three values). The height of the specimen was carefully measured using a vernier calliper.

The samples were saturated by first flushing with carbon dioxide (CO_2) for about 45 minutes. Then de-aired water was passed slowly through the samples until no air bubbles were observed coming out from the outlet pipe. A backpressure of 200 kPa was then applied to saturate the soil sample. For very dense samples, a higher backpressure of 300kPa was applied. All samples were considered to be fully saturated when the Skempton pore pressure ratio was at least 0.95. The samples were consolidated at the target effective

confining stresses of 50, 100, 150, and 200 kPa until no significant volume change was detected. Bender element tests were performed at the end of the consolidation at each stress state. The height change and volume changes for saturated specimens were captured automatically by the transducers. Figure 6 shows the schematic diagram of the testing equipment.

3.7 Signal interpretation – Bender Element

The start-start method was chosen to determine the travel time for the kuroboku soils, similar to Nishimura (2006) for London Clay and Yang and Gu (2013) for fine glass beads. Sine waves with a wide range of excitation frequencies (2–20 kHz) were initially used as input signals for the BE tests. A frequency of 8 kHz was chosen to determine shear velocity, V_s since it was found that the near field effects were negligible above this threshold. It is noteworthy to highlight that Nishimura (2006) also used a similar frequency for the input wave for London Clay (9 kHz in his case).

By appropriately interpreting the waves, V_s may be evaluated from which G_{max} can be determined. The shear velocity could be estimated by the following equation:

Shear wave velocity: $V_s = \frac{L}{\Delta t}$ (1)

where

L: length between tip to tip of bender elements (mm) and

Δt: shear wave travel time (ms)

The shear stiffness modulus may then be estimated using the following relation:

$G_{max} = \rho V_s^2$ (2)

where

ρ: bulk density

3.8 Electron microscopy analysis

The soil fabric was studied using both a scanning electron microscope and a field emission microscope. Low Vacuum High Sensitivity Scanning Electron Microscope (SEM), Hitachi SU3500 was used to view the silt and sand sized components of the soil.

Allophanes and imogolites are nano-sized particles and thus Field Emission Scanning Electron Microscope (FE-SEM), Hitachi SU-8000 was used to capture their pictures. Some modifications were brought to the sample preparation method proposed by Pérez *et al.* (2016) to view the nano-sized particles. About 0.4g of each soil material was placed in a 50ml glass vial, which was then half filled with distilled water. After that the samples were left to soak for a day before being given a sonication bath for 20 min. The glass vials were

then left to stand for roughly 10min, during which the suspension were about clear. Using a dropper pipette, a minute sample was collected from the upper portion of the suspension. The drop was carefully placed on a small piece of aluminium foil which had been laid in a paper tray and sleeve box and left for drying. Aluminium foil was chosen instead of sample holders as the latter have conical troughs and the dried samples might congregate, making it more difficult to observe the nano-particles. The sleeve box was used to prevent contamination of the sample. Soils have poor conductivities and charge can accumulate which would lower the image quality. Thus, the dried soil samples on the aluminium foils were sputtered with osmium, prior to carrying out the microscopy analysis.

4. Results and discussions

4.1 Microstructure

Improvement in microscopy techniques allowed researchers to rectify the initial presumption that allophanes were not amorphous material but actually short ranged aluminosilicates. Levard *et al.* (2012) mentioned that allophanes are not easy to discern and that there is a dearth of clear images to identify their "well-defined ring-shaped structures". These claims seem justified from the premise that conceptual models have been proposed based on images of pre-treated soil samples obtained from Transmission Electron Microscope (TEM). Images of untreated soil specimens would most likely further enhance our knowledge about the microstructure of this clay material.

In this endeavour, using FE-SEM images of untreated samples, the microstructure of the kuroboku soil was assessed according to three factors: (i) soil constituents; (ii) contact relation and (iii) pore characteristics.

4.1.1 Soil constituents

The main components of the black volcanic ash are clay minerals like allophane and imogolite in addition to volcanic glass and feldspar plagioclase. Particles smaller than 75μm account for more than 90% of the total constituents of all the soils except for Soil 2B, where the figure stood at just under 80%. Wada (1978) mentioned that compounds like SiO_2, Al_2O_3 and Fe_2O_3 make up more than 90% of allophanic soils. X-ray fluorescence tests on Soil 2 showed that the percentage by weight composition for SiO_2, Al_2O_3 and Fe_2O_3 were respectively 50.5, 28.9 and 14.1. This gives an SiO_2/Al_2O_3 ratio of 1.75 corresponding to a high allophanic material according to Henmi and Wada (1976).

4.1.1.1 Observations by SEM (Assemblage level)

Using the terminology of Collins and McGown (1974), at the assemblage level, agglomerated particles together with volcanic glass and plagioclase particles could be observed. The aggregated particles were mostly clothed silt or sand sized particles. The volcanic glass shards were generally porous and vesicular in nature, displaying irregular edges with conchoidal fractures. Authigenic clay formation could also be observed on the surface of some volcanic glass. Few were the volcanic shards that displayed clean surfaces with most showing much surface degradation probably as a result of violent eruption and weathering (Figure 7(a-1), 7(d-1), 7(e-1) and 7(g-1)).

From Figure 7(a-1), the regular aggregates in Soil 1 which were about 200 x 200μm (fine sand size) could be observed. Considering the SEM images of Soil 1C (Figure 7(d-1), it could be inferred that the regular aggregates from Soil 1, in most cases, were clothed silt sized volcanic glass particles. A few spheroidal particles (20μm in diameter) were observed in Soil 1 (Figure 7(a-1)). Smaller volcanic glass were also conspicuous. Compared to Soil 1, Soil 2 displayed more isolated and coarser volcanic glass particles. Medium sand size (300μm) volcanic glass roughly 50μm thick was observed in Soil 2 (Figure 7(e-1)). While we testified that the maximum sizes of regular aggregates were typically fine sand size (200μm), but compared to Soil 1, their relative abundance was smaller. Soil 1C showed coarse silt and a little fine sand size volcanic glass (40 - 100μm) with some clay material sticking on the surfaces or filling the pores. These volcanic glasses were actually coated with clay particles and the sieving process allowed us to appreciate this feature.

Soil 2B, which was obtained by air drying, had fine sand sized aggregates and volcanic glass particles with sizes varying between 60 and 150μm. It seemed that the process of aggregation (due to drying) enmeshed smaller volcanic glass within the clay material, leaving out larger particles of volcanic glass. Soils 1A, 1B and 2A had fewer volcanic glass particles which were respectively less than 50μm, 38μm and 75μm (Figure 7(b-1), 7(c-1), and 7(f-1)). The aggregates were also smaller than soils 1, 1C, 2 and 2B. Compared to Soils 1A and 1B, the volcanic shards in Soil 2A appeared more vesicular and porous.

In comparison with the allophanic volcanic ash tested in this study, Sorem (1982) reported that dacitic volcanic ash from Mt. St. Helens had larger composite ash clusters which ranged from 250 to 500μm in diameter (medium sand size). Silt sized volcanic glass between 20 and 40μm made a big chunk of these ash clusters. Like the volcanic shards in this study, Sorem (1982) observed that the volcanic glass showed vesicles and conchoidal fractures.

Similar to the kuroboku soil, for rhyolitic volcanic ash from New Zealand, Moon *et al.* (2015) mentioned the conspicuous presence of volcanic glass. These shards were however reported to be mostly clean unlike the materials used in this study. Plates were more common in the rhyolitic ash. Both Cunningham *et al.* (2016) and Moon *et al.* (2015) mentioned the presence of halloysite books commonly between 1.5 and 50μm with some unusually big with sizes up to 1.5mm reported. These types of particles were not observed in the kuroboku soils.

4.1.1.2 Observations by FE-SEM (Elementary particle level)

The FE-SEM images help us grasp the features at the elementary particle level arrangement. One of the glaring observations from the FE-SEM images was the distinct presence of allophane and imogolite clay minerals in the soils tested. The FE-SEM images indicated that the allophane domains had not been much affected from remoulding as a result of the sieving process. The internal water in the stiff individual spherules was thus still present despite remoulding.

The smallest "fluffy" allophane domains observed were about 9nm (Figure 7(c-3)) while 195nm large domains were also seen (Figure 7(f-2)). Spherules of 3.5nm or 5nm were not observed. It could be that in the present configuration, with the strong flocculating tendencies of the soil, formation of small size domains of about 9nm was favoured. It could also be that sonication alone was not enough to overcome the strong electrostatic attraction (intra-particle bonding) aggregating the individual spherules together. Figures 7(c-2) and 7(c-3) allow us to understand the infamous TEM image of pre-treated and dispersed allophane and imogolite samples obtained by Henmi and Wada (1976). We may reasonably deduce that the micrographs obtained by these researchers are actually flattened allophane domains covered by imogolite fibres. From Figure 7(c-3), it can also be seen that together the allophane domains and imogolite fibres may occasionally depict a morphology akin to an inverted micelle. These features may not be readily observed from dispersed samples and to the best knowledge of the authors have not been highlighted previously. It can be further speculated that the imogolite fibres between allophane domains were formed after the latter. This observation supports the genesis sequence of imogolite postulated by Henmi and Wada (1976). Moreover, the allophane domains assume both spheroidal and ellipsoidal shapes. The ellipsoidal domains may be an indication of the ongoing process of aggregation.

The noticeable presence of imogolite fibres meshing around allophane particles and volcanic glass could be observed in all soils except for Soil 2B. The imogolite bundle on the array of allophane domains could be estimated to be around 10 to 20nm thick (Figure 7(c-3)), while the thinnest imogolite thread connecting the individual domains could be estimated to be around 3.5 nm. According to Wada *et al.* (1970) imogolite always occur in pair, so that the thickness of an individual fibre could be estimated to be about 1.75nm.

Platy-shaped particles were also observed. The size of the plate observed in Soil 1 (Figure 7(a-4)) was about 8 x 5 μm. No opaline silica in its usual ellipsoidal form was identified although they may have been broken down into smaller pieces.

Figure 7(e-2) shows a 165x185nm spherical halloysite particle in Soil 2. The relative abundance of these spherical particles in Soil 2 seemed low and they were not observed in Soil 1, 1A, 1B and 1C. Given that the tubular spikes usually associated with halloysites were not observed, it could be that these particles are at an early stage of their genesis. Soil 2 from which spherical halloysites was observed, was collected just off the Aso bridge landslide site. Presence of spherical halloysites has been associated with landslides (Smalley *et al.*, 1980; Tanaka, 1992; Moon, 2016). Yoshinaga (1986) had reported increasing halloysite content with burial depth for a pedon taken from a plot of land about 5km from Site 2. Further studies on the possible influence of the spherical halloysites into landslides in this area may be warranted.

Figure 7(b-2) shows a pennate diatom observed in Soil 1A. The surface of the diatom frustule is indicative of a highly porous and rough material. The diatom seems to have been broken close to its central nodule. Thus, we estimate the full size of the diatom to be about 3.3 x 13μm (medium silt size). Similarly we observed diatoms in Soil 1 (Figure 7(a-4)), Soil 1B and Soil 1C (although the relative abundance in Soil 1C was lower). Sieffermann and Millot (1969), Mizota *et al.* (1982) and Verdugo (2008) previously reported the coexistence of allophane and diatoms. Mizota *et al.* (1982) stated that the presence of diatoms in andosols may be an indication of an early stage of soil development or paddy type soil conditions.

In Soil 1C even if granular materials increased after the sieving process, the microstructure was still governed by the clay matrix. The photo of Soil 1C in Figure 7(d-2) shows some resemblance to the micrograph of a remoulded allophanic soil from Waitui site in New Zealand that had been examined by Jacquet (1990). Jacquet posited that the original structure of the soil in Waitui had been destroyed, rendering the imogolite to a “featureless gel”. In this study, we only observed this abrasion of imogolite fibres in Soil 1C, which it has to be said was not was not as wholesome as in the case of the Waitui site. Part of the fabric still showed imogolite with what could be described as minimal alteration.

From the observations made in Figure 7(g-2), it could be confirmed that the effect of drying led to the dehydration of the imogolite fibres, creating a flaky material. The domains still retained a general stiffness. Nonetheless, the way the domains were lined up, could signify that the drying process led to the contraction of their volume. This may be well observed from Figure 7(g-3), for which the colours and hues were adjusted to better appreciate these features.

4.1.2 Contact relation

The interaction between the volcanic ash particles is a function of the configuration and shape of the various soil components. Since the kuroboku volcanic ash is an aggregate dominant soils, face to face contacts are most likely. With face to face interaction, the amount of bond at contact would be larger. Some grain to grain contacts between solid particles like volcanic glass or feldspar plagioclase is expected in Soil 1C and Soil 2 (Figures 7(d-1) and 7(e-1)). Direct contact between the volcanic glass is not commonplace in soils 1, 1A, 1B and 2A and more likely to be interfered with clay particles. Point to point contact between the spheroidal particles in Soil 1 (Figure 7(a-1)) appears unlikely given their relatively low abundance. From the micrographs, it did not appear there was any bonding between the solid particles and clay materials.

Soil 2B is mostly made up of aggregates and individual volcanic glass particles with very little "free" clay particles. Thus, grain to grain contact may be equally as likely as face to face contact in Soil 2B (Figure 7(g-1)). In some cases, the grain to grain contact in Soil 2B may be similar to the interlocking contact typical of loess soils. Particles with a platy shape seemed to occupy a very small volume, such that edge to edge and edge to face contacts may only be possible locally where some clustering between the plates occur.

In contrast with the kuroboku soil, the grains in the dacitic volcanic ash from Mt. St. Helens interact mostly through particle to particle contact (Sorem, 1982). The grain contacts were described as being clean and sharp, with no evidence of cementation. Same as for the kuroboku soil, Moon *et al.* (2015) mentioned that the clay minerals get in the way of solid particles like volcanic glass, such that grain to grain contact were rare. Platy particles were more common in the rhyolitic ash from New Zealand. Edge to edge or edge to face arrangements were observed between them. The tubular halloysite particles mostly interact through point contacts. There was little indication of bonding between the clay minerals and the granular soil components similar to the kuroboku soil and the volcanic ash from Mt. St. Helens. Moreover, all these soils are characterized by an open structure.

4.1.3 Pore characteristics

From the micrographs, it was observed that the soil structure consisted of different types of porous particles (allophane, imogolite, diatoms, plagioclase, volcanic glass and so on) in different configuration and at different internal spatial scales (including individual elements, aggregates, filiforms, clusters and domains). This largely explains why the volcanic ash are very porous with maximum void ratios of about 5.

The terminology proposed by Collins and McGown (1974) was adopted to describe the pore types in the kuroboku soil. The list include intra-elemental (interparticle & intergroup), intra-assemblage, inter-

assemblage and transassemblage pores. As for the pore sizes, the classification system of the International Union of Pure and Applied Chemistry (IUPAC) was used. Micropores have sizes smaller than 2nm, mesopores are between 2nm and 50nm while macropores are larger than 50nm.

The largest pores (macropore) that would occur in the field would be of the transassemblage type as a result for example of roots, wormholes or rodent holes. The other macropores (intra-elemental pores) occurs within solid particles (like volcanic glass and diatoms) and in the spaces due to the latter's fractured surface (Figures 7(a-1), 7(b-3), 7(d-1), 7(e-1) and 7(g-1)). Relatively big intra-elemental pores could be observed in the volcanic shards of Soil 2. Site 2 lies on the western side of the Aso caldera. The prevailing wind in the area is westerly (Wada, 1985). Thus, it is quite reasonable to infer that particles on the west side of the caldera are products of more violent eruptions and hence are likely to be more porous. In comparison to Soil 2, the volcanic glass in Soil 1C (and by extension in Soil 1) appear to be less porous with fewer and smaller intra-elemental pores.

In addition abundant macropores (inter and intra-assemblage pores) could be observed within and around the clay clothed (volcanic glass) aggregates (Figure 7(a-1), 7(b-1), 7(c-1), 7(d-1), 7(e-1), and 7(g-1)). Macropores occurring as a result of interlocking (interparticle pores) were visible in Soil 2B (Figure 7(g-1)), but almost inexistent elsewhere. Interlock pores are commonly observed in loess soils and have been reported as being responsible for their collapsible nature. It should be mentioned that it was difficult to prepare loose samples (void ratio greater than 4) for Soil 2B in comparison to other soils. In fact, Soil 2B is expected to be less stable in the loosest state with the lack of finer particles to fill the interspaces.

Mesopores could be found between allophane domains (intergroup or inter-pedal pores), between imogolite threads and within diatoms. From Figure 7(c-3), inter-pedal pores under 10nm could be observed between allophanes domains while inter-thread pore of 7nm was also identified between imogolite fibres. Mesopores of about 16nm and 30nm could be viewed in the pennate diatom in Figure 7(b-3). Micropores are expected to be found within and between the domains of allophane and both in the intra and inter thread pores of the imogolite. However, these could not be readily observed from the FE-SEM images.

4.1.4 Conceptual microstructure model

The microstructure of the allophanic soils was described in the foregoing subsections. From the above discussions, representative conceptual microstructure models were proposed in Figure 8. The following elements may be highlighted.

Soil 1 (Figure 8 (a)) is made to a great extent of fine sand size volcanic glass, which are mostly clothed particles with small intra-elemental pores. The composite microfabric display a rather continuous assemblage network. Blow up within clay aggregate show the presence of diatoms, allophane and imogolite. In contrast, Soil 2 (Figure 8 (b)) has medium sand size volcanic shards with relatively larger intra-elemental pores. The latter locally create a fragmented assemblage network. Soil 2B (Figure 8 (c)) consist of dried clay aggregates and the volcanic glass can combine under external force creating interlocking pores. Figure 8 (d) highlights the contact relation in Soil 1C under isotropic mean effective stress. The three possible contact types were (i) face to face contact between clay aggregates or clothed volcanic glass particles; (ii) buttress type contact between thinly clothed volcanic shards and (iii) clean (grain to grain) contacts. The representative conceptual microstructure units for soils 1A, 1B and 2A would essentially be a scaled-down model of their parent material.

It is difficult to generalize a conceptual model for volcanic ash, the composition of which varies with factors like nature of eruption, deposition environment, mineralogy, age of deposits and weathering. Moreover, volcanic ash containing allophane and halloysite minerals are grouped as a distinct category of residual soil, which usually do not show effect of macrostructure unlike highly weathered rock (Wesley, 2010). Hence, the conceptual model may be limited to volcanic ash containing allophane or halloysite. Features that would equally apply may include, the tendencies for the clay minerals to form aggregates, the contact relations and formation of interlock pores. What will differ is the presence of specific elements within the aggregates. For instance, presence of diatoms or halloysites which can assume different morphologies including tubular or books which were not observed in this study. Also the degree of alteration of the volcanic shards may depend on the nature of volcanic eruption or degree of weathering.

4.2 Influence of characteristics of allophane on grain size distribution and liquefaction susceptibility

4.2.1 Grain size distribution

While carrying out the grain size distribution, the same difficulties in preventing the soil particles from re-flocculating that was mentioned amongst others by Wesley (1973), Maeda *et al.* (1977), Rouse *et al.* (1986) and Jacquet (1990) was encountered in this study. According to Wells and Theng (1985) who studied the flow behaviour of allophanic soils from New Zealand, the main reason for the strong flocculating nature of allophane particles is the existence of strong intra-particle (primary) bonds due to electrostatic attraction. Hydrogen bonding around the allophane particles and adsorbed hydrous iron oxides in addition to inter-

particle Van der Waals and hydrodynamic forces (secondary bonds) further enhance the flocculating tendencies.

The degree of flocculation is highly dependent on the pH of the soil. From the study of Wells and Theng (1985) maximum flocculation was found to occur at the point of zero charge (PZC), which corresponded to a pH of 5.5 to 6.5. Similarly, Nakagawa and Ishiguro (1994) investigated the effect of acid rain on the dispersion of allophanic andosols. From their results, it could be deduced that the soils were least dispersed between a pH of 5 to 9.

Yamada *et al.* (1969) as cited by Sudo (1978) mentioned that allophane occur in soils associated with ground water that has a pH in the intermediate range. For soils near to site 1, Kubotera *et al.* (2013) reported that the pH in H_2O was between 4.03 and 6.13. In our study, the pH in H_2O, for soils 1 and 2 were 4.9 and 5.5 respectively. Hence, both soils would show strong flocculating tendencies. As a result, the graphs obtained by the laser method (Figure 9), actually, represents the "aggregate" size distribution. Some improvement in dispersing the particles was observed when using sodium hexametaphosphate for the hydrometer analysis. A question, then, that ought to be asked is how relevant is the particle size distribution for allophanic soils. For argument sake, it is common knowledge that the effective size, D_{10} value is used in correlation formulae for estimating the permeability of soils (like in Hazen's formula). But allophanic soils are likely to display dual porosities as a result of inter-assemblage and intra-assemblage pores (Zhang, 2007) and in turn, this characteristic would influence the permeability. Hence, it would seem that the main purpose of dispersal of allophanic particles would be to get a realistic estimate of its clay size fraction. But other than that how useful would other indices like D_{10} and mean particle size, D_{50} be if deduced from the dispersed particle size distribution. This point would be worthy of further investigation.

4.2.2 Liquefaction

After the 2016 Kumamoto Earthquake, Kayen *et al.* (2017), Chiaro *et al.* (2017), Hazarika *et al.* (2017), Kayen *et al.* (2018) and Ogo *et al.* (2018) carried out field reconnaissance surveys at the affected areas. Based on their observations and experience, they concluded that for a series of high intensity earthquakes that occurred within a short lapse of time, in an area with rather high ground water table, the number of liquefaction sites was relatively small. Kiyota *et al.* (2017) also reported that there had been "no official report of serious liquefaction-induced damage" and overall the number of damaged buildings and other amenities was much less compared to the Kanto areas during the 2011 Tohoku Earthquake.

The highest Peak Ground Acceleration (PGA) recorded (at Mashiki Town) was 1399 Gal (UD) for the foreshock event (14 April 2016) and 1157 Gal (EW) for the mainshock event (16 April 2016) (National

Research Institute for Earth Science and Disaster Resilience (NIED), 2022). As a means of comparison, information about the PGA of some historical earthquakes that induced liquefaction damage have been compiled in Table 3. Ishihara (1985) had proposed boundary curves for site identification of liquefaction - induced damage (Figure 10). According to Youd and Garris (1995), this chart performs reasonably well for cases where no lateral spread is observed. van Ballegooy *et al.* (2015) also said that Ishihara's chart are "conceptually correct" with a limitation observed in highly inter-bedded soil strata. Kayen *et al.* (2017) suggested that the Kumamoto Earthquake may be a case of zero displacement lateral spread. Hence, from a cursory assessment of Ishihara's chart we can understand the claims of Kayen *et al.* (2017), Chiaro *et al.* (2017), Hazarika *et al.* (2017), Kayen *et al.* (2018) and Ogo *et al.* (2018) that much more liquefaction ought to have been expected for such a high PGA.

Based on data from Chiaro *et al.* (2018b), the point corresponding to the liquefaction of the pumice layer at the Takanodai landslide site was also added to Ishihara's chart. The 8.6m of surface, non-liquefiable allophanic soil was composed of alternating layers of kuroboku and akaboku soils (red allophanic volcanic ash). The PGA at the closest seismograph to the Takanodai site was 526 gal (NS), with the three vector component being 669 gal. The point for the Takanodai may seem slightly off the "400-500 gal" curve proposed by Ishihara from data of the Tangshan Earthquake. But it should be highlighted that the Takanodai site had an initial slope of about 12-15° with the angle of the potential slip surface estimated to be about 6° (Chiaro *et al.*, 2018b), giving the incipient failing mass of earth a downward acceleration.

Kayen *et al.* (2017) posited that the plasticity of the volcanic soils or significant presence of a clay content as possible reasons behind the paucity of liquefaction. They can also be quoted as saying that "given the scientific importance associated with this lack of understanding", further studies would be needed to determine the reasons for the unusual observations.

Liu (2019) carried out cyclic triaxial tests in two stages (1^{st} liquefaction $\xrightarrow{\text{reconsolidation}}$ 2^{nd} liquefaction) on remoulded kuroboku soil from Site 2 (from a different sampling spot) and Toyoura sand. The initial void ratio of the soil was 3.1. With the failure criterion set at double-amplitude (DA) strains of 5%, at an effective confining pressure of 50kPa, it was observed that the liquefaction resistance of kuroboku soil was appreciably higher than Toyoura sand. The results of the cyclic tests have been reproduced in Figure 11. For the natural kuroboku, at the end of the first consolidation stage the void ratio was 1.28 representing a very dense condition. Since the liquefaction resistance of the natural kuroboku was very high, fines were removed. Samples of washed kuroboku (with fines content of about 25%) and Toyoura sand with a common relative density (D_r) of 60% (corresponding to in-situ D_r) were thus prepared. Owing to the influence of electrostatic bonding and imogolite fibres, mechanical action was needed to remove the fines. In real situations, even in

extreme rainfall conditions, it is improbable that so much fines would be washed away. Hence, the "washed fines" samples at D_r = 60% represents a worse situation than in-situ conditions. The liquefaction resistance of the washed kuroboku was still much higher than that of Toyoura sand.

Studying undisturbed allophanic volcanic ash from Chile, Verdugo (2008) also observed the high cyclic resistance of this type of soil. He stated that this material may not liquefy even in the strongest of earthquakes. The liquefaction resistance of allophanic soils may decrease if the materials yield or as a result of ground contamination which causes the pH of the soils to become more acidic or alkaline. From Figure 11, it can be further observed that overall, the cyclic resistance of the allophanic kuroboku and Santa Barbara soils are comparatively higher than coarse grained volcanic soils and pumice sand reported by Miura *et al.* (2003) and Watabe and Nishimura (2020) respectively. It should be noted that in their work Miura *et al.* (2003) had compared the cyclic strength of reconstituted coarse volcanic soils (roughly at in-situ density) with dense Toyoura sand (D_r = 80%).

Liu (2019) suggested high fines content as a possible explanation for liquefaction resistance. A step further, it is believed that the reasons for the liquefaction resistance lies, to a great extent, in the nature of the allophane particles (which make up the "fines"), in particular, the surface properties of the allophanic particles and the strong electrostatic bonding existing between them. When the pH of the soil is close to the PZC, owing to the surface properties, interaction between allophane particles is enhanced which mobilizes a high viscous resistance. In addition, much external force is required to overcome the strong electrostatic attraction between the allophanic particles. This is exemplified in Figures 7(a-4), 7(a-5), 7(a-6) and 7(a-7) from which it could be observed that despite sonication, it was difficult to separate the allophane domains to their individual spherules. Wells and Theng (1985) stated if an aggregated soil material shows resistance to ultrasonic vibration, it would likewise prove to be shear resistant. Besides, the imogolite fibres weaving around the allophane were still attached to a platy-shaped particle. Wells *et al.* (1980) mentioned that imogolite threads enmeshing around the allophane domains creates a network which gives further resistance during moderate shear because of interlocking. The increase noted in the cyclic resistance for the second stage of liquefaction for the kuroboku soils, may not be limited to increase in density but may also be the result of the effects of structuration. The enhanced entanglement of imogolite fibres in the denser material from the first stage of liquefaction coupled with the strong electrostatic bonding in the allophane particles, at an effective confining pressure lower than the yield stress improved the liquefaction resistance.

Based on information available from NARO (2022), an indicative map of the coverage of allophanic soils in Kumamoto and Oita prefectures was prepared (Figure 12). The ubiquitous presence of allophanic soils can be confirmed, especially around the central areas of these prefectures which are associated with higher

rainfall. The sites where sand boiling had been observed by Wakamatsu *et al.* (2017b) after the Kumamoto Earthquake, were also superimposed.

Four clusters may be defined for places where sand boiling was observed. Cluster 1 denotes the areas around and along Shirakawa and Midorikawa rivers and Kumamoto port, Cluster 2 represents the region around the port of Yatsushiro, while Cluster 3 and Cluster 4 designate parts of Aso City and Minami Aso respectively.

Mukunoki *et al.* (2016), Hazarika *et al.* (2017) and Wakamatsu *et al.* (2017b) all concurred that most locations of liquefactions coincided with reclaimed lands, river embankments, former stream channels and flood plains. It can be further observed in Figure 12 that for clusters 1 and 4 the sand boiling locations lie mostly outside the areas covered by allophanic soils. Where sand boiling was observed in allophanic soil areas (within these two cluster groups), most of the locations fell along the sides of rivers and were largely part of existing embankments.

Wakamatsu *et al.* (2017b) mentioned that sand boiling in Aso city (cluster 3), around Goshi, Otsu and Kikuchi occurred after the mainshock. Wakamatsu (2017a) stated that in Aso city, there had been no report of major liquefaction related damages to houses. Liquefaction effects (sand boiling) was limited to agricultural land and facilities (farm roads, waterways, etc.) and some river embankments. Pedon P3 from Wada (1986) in Aso city was taken from a paddy field site, with the upper horizons dominated by diatoms and goethite and the lower horizons by allophane and diatoms. Otowa (1986) reported that the upper soil stratum was not well drained with gray subsoils and presence of tubular iron mottles. These elements may have had some bearing in that surficial effects of liquefaction in terms of sand boiling was observed in parts of agricultural lands. In Central Aso City (Yakuinbaru) sand boiling was observed in some agricultural plots composed of allophanic material. Wakamatsu (2017a) provided evidence from old maps that a water course ran through this area and had been reclaimed around years 1953 to 1966.

The sand boiling observed in Goshi, Otsu and Kikuchi may be considered as sparse. As was mentioned at section 3.2, the ejecta from Mt. Aso are characterized by varying composition such that local lithology may have some influence on these observations. For instance, the pedon data (P1) from Wada (1986) revealed somehow uncharacteristically that halloysite soils of 1.3m thickness (upper soil horizon) overlaid allophanic soils. However, a few kilometres east at pedon P2, allophane is the dominant clay material in the first two metres of soil. Yoshinaga (1986) attributed the presence of allophane in lower soil horizons to the different nature of parent tephra compared to the upper horizons.

From historical records, it could be deduced that after the 1889 Kumamoto Earthquake, liquefaction also occurred outside the areas covered by allophanic soils (Kuribayashi and Tatsuoka, 1975). The locations

coincided with cluster 1 and areas between Hikawa and Uki as shown in Figure 12. From the discussion in this section, it is believed that the localities found on allophanic lands are at a lower risk from liquefaction induced damage.

The Overseas Coastal Area Development Institute of Japan (2009) proposed grain size distribution limits for prediction and judgement of liquefaction susceptibility. As can be observed from Figure 9, the grain size distributions of soils 1 and 2 lie largely within the zone of possible liquefaction. In view of the strong flocculating tendencies in field conditions coupled with resistance to sonication, it is expected that even after an earthquake the grain size distribution would remain to a great extent within the bounds of the possible liquefaction range. Taking into account the resistance shown to liquefaction by the allophanic kuroboku soils in the cyclic tests, corresponding judgement based on the grain size distribution may be flawed. From our observations described herein and in section 4.2.1, there are reasons to agree with Rouse *et al.* (1986) that allophanic soils may not be amenable to classification through grain size distribution. Instead of grain size distribution, recognizing the predisposition of allophanic soils towards liquefaction, it would be more relevant to assess the stratification of the liquefaction resistant allophanic soils with liquefiable soil layers.

4.3 Influence of void ratio and effective confining pressure

Figures 13(a-g) and 14(a-g) show the relationship of void ratio and effective confining stress with respect to the small strain shear modulus for all the soils tested in this study. It should be highlighted that the soils in their two densest states were prepared from samples below the water content threshold mentioned at section 3.5. Moreover, the void ratio in all these figures are those after consolidation and at the instant the BE tests were performed. The initial void ratios of Soil 1 and Soil 2 were respectively about 3.7 and 3.8. As can be observed, at a given effective confining stress the shear modulus decreases with increasing void ratio, and for a given void ratio the shear modulus increases with an increase in effective confining stress. These results concur with the findings of other researchers like Iwasaki and Tatsuoka (1977), Sahaphol and Miura (2005), Wichtmann and Triantafyllidis (2009), Liu *et al.* (2016), Okewale and Coop (2017) and Okewale and Grobler (2020).

As Senetakis *et al.* (2012) reported, the main reasons for these observations were the development of normal forces of higher magnitude at particle contacts with increasing effective confining stresses and denser packing of the soil particles.

4.4 Variation of G_{max} among the soils

For the same effective confining pressure, when the graphs of G_{max} of the various soils are plotted together (Figures 15(a-d)), it can be appreciated at face value that the variation in small strain shear stiffness among all the soils tested is quite small. Nonetheless, delving into these slight differences allows us to appreciate the contribution of the various components of the soils and their associated interactions. In general, at equal void ratios, the small strain stiffness was greatest for Soil 1, followed by Soil 2, Soil 1C and the other soils. Using Fourie *et al.* (2012) terminology, the main reason for this pattern lies in the strength of the composite microfabric.

Santamarina *et al.* (2001) mentioned that the stiffness is contingent on the strength of the aggregates and/or particles and the contact relation. Skeletal forces control the deformation at contacts for coarse grained particulate materials according to the theories developed by Hertz and Mindlin. However, for fine soils, electrostatic force also exert a strong influence, especially for soils with minerals that have high specific surface areas like allophane. In effect, the electrostatic forces which stem from oppositely charged defect sites on the allophane particles determine the strength of the aggregates. These electrostatic attraction are contingent on environmental variables like pH. As was mentioned at section 4.2.1, with the pH in H_2O, for soils 1 and 2 being close to the PZC, strong electrostatic attraction would prevail. It is therefore expected that at a macro level the conglomerates would be relatively stiff such that the soil would behave like a pseudo granular material (Rao, 1995). In this study we used saturated soil samples, so capillary forces may not be relevant.

At a micro level, though, it is a major challenge to determine the contact and non-contact conditions (Santamarina *et al.*, 2001). Pre-treatment with chemicals and sonication is needed to overcome the electrostatic forces and observe the individual allophane spherules which have a dimeter of 3.5 to 5nm. In real case, it has yet to be confirmed visually how the individual allophane spherules actually make contact given that the prevailing long range attraction and repulsion forces can project a greater distance from the allophane particle in comparison with the latter's size.

Allophane are hollow spherules that hold water. Shear waves normally do not propagate through liquids. Hence, it might be expected that the shear waves would move along the shell of the spherules. The same principle is likely to apply to imogolite fibres. Allbrook (1985) had mentioned that allophane remain as discrete particles. However, from our observations on untreated samples, formation of domains were favoured with the strong electrostatic attraction. Karube *et al.* (1996) posited that the individual allophane particles could interact as a string of beads in the domains. The way the dehydrated allophane spherules

were lined up in Figures 7(g-2) and 7(g-3) may lend support to this hypothesis. However, it is not known how the space not occupied by individual allophane spherules is actually filled up within the domains. There can be a mobile fraction that is not affected by external load. As observed in Figure 7 (c-3) and described at section 4.1.1.2, the allophane domains remain in a latent phase of change, aggregating to larger domains or clusters which assume various morphologies. Hence, these domains and clusters may not be strictly particulate and could break down into smaller particles depending on the magnitude of external force applied.

The presence of multiple internal scales (individual elements, aggregates, filiforms, clusters and domains) and how they interact adds to complication in the study of the fabric of fine soils (Bennett & Hilbert, 1986; Santamarina *et al.*, 2001). Santamarina *et al.* (2001) therefore suggested that the interaction between the soil constitutents in a fine grained soil like allophanic volcanic ash be described at two different scales, namely at the assemblage and elemental level. In the following subsections, we describe the possible influence of the composite microfabric, components like diatoms and imogolite and features like the intra-elemental pore on the difference in small strain shear stiffness noted above.

4.4.1 Characteristics of composite microfabric and contact influence

Compared to Soil 1C and Soil 2, it may be inferred that the composite microfabric of Soil 1 displays a rather continuous assemblage network (Figure 7(a-1) and 7(e-1)). As mentioned previously at 4.1.1.1, Soil 2 has more isolated and coarser volcanic glass particles than Soil 1. Upon saturation and application of external load, the clay minerals would weakly wrap around these isolated volcanic shards. Hence, at the composite level of fabric organization, these loosely covered volcanic glass would locally interrupt the assemblage network, giving rise to an “embedded system”.

The same “embedded system” features in Soil 1C. Moreover, in Soil 1C, the contact relation of the particles was also altered with the sieving process. As a result, we have varied contact types in Soil 1C, ranging from clean and clothed contacts. The clothed contacts in some spots may only act as buttress (less effective bonding - Figure 8(d)). At very high effective confining stresses, the volcanic glass would be crushed and it may be expected that the small strain stiffness of Soil 1C and Soil 1 would converge to a common value.

The volcanic glass particles in soils 1A, 1B and 2A are smallest and also occupy a relatively small volume, such that they appear to be floating among the volcanic ash particles. Thus, the composite fabric is expected to be weaker even with the close arrangement of the particles. The small strain shear stiffness of Soil 2B is relatively low at effective confining stresses of 50 and 100 kPa, but progressively rises with enhanced contact at higher effective confining pressures.

4.4.2 Influence of diatoms at low effective confining stresses

From Figure 15(a), it can be observed that at an effective confining stress of 50kPa, the difference in small strain shear stiffness between Soil 1 and Soil 2 was greatest, with Soil 1C showing nearly the same value as Soil 2. Furthermore, at this very effective confining stress, the small strain shear stiffness of soils 1A and 1B were distinctively above that of Soil 2A and very similar to that of Soil 2B. The reason for these observations probably lie in the presence of diatoms in the kuroboku soil sampled from Site 1.

Day (1995) carried out stimulating work on diatomaceous fill. From it, we understood that diatoms may provide additional strength at low effective confining stresses (50 kPa) because of their roughness and through interlocking. At higher effective confining pressures, the contribution of diatoms to small stiffness fades as they become a compressible material by crushing (Figures 15(c) and 15(d)).

4.4.3 Intra-element pores as weak spots

The volcanic glass in Soil 2 and its derivatives show larger intra-element pores compared to Soil 1. The larger intra-element pores are probably the result of violent eruption and represent a point of weakness as explained at section 4.1.3. It is very likely that the volcanic glasses in Soil 2 would be more brittle and crushable. From this perspective, the contribution of volcanic glass to the small strain stiffness in Soil 2 would be slightly less compared to Soil 1.

To further illustrate this point, we can look at the magnitude of the stress components for the effective confining pressure. Sahaphol and Miura (2005) and Asadi *et al.* (2020) used the following general equation to relate the void ratio, e and effective confining stress, σ' with the small strain shear modulus, G_{max}:

$$G_{max} = A(e)^{m}(\sigma')^{n} \qquad (3)$$

Figure 16 shows how the stress components m and n compared for each soil tested in this study. The stress exponents of some soils used by Sahaphol and Miura (2005) and Asadi *et al.* (2020) have also been included. Sahaphol and Miura (2005) determined that the n values for Kitami, Mori and Touhoro soils were 0.56, 0.60 and 0.70 respectively. Asadi *et al.* (2020) mentioned a value of 0.59 for a natural pumiceous sand (NP3) from New Zealand and 0.5 for the standard Toyoura sand. According to Sahaphol and Miura (2005) and Asadi *et al.* (2020), a higher n value is an indication of a more crushable material.

The n values of Soil 2 and its derivative soils (2A and 2B) were higher than that of soil 1, 1A, 1B and 1C. The n value for Soil 2 at low stress levels (50-100kPa) was 0.53. This was higher than that of Soil 1 at high stress levels (150-200kPa), for which the n value was 0.50. From this higher dependency on effective confining stress, it could be inferred that Soil 2 was more compressible than Soil 1. This is a direct

consequence of the larger intra-elemental pores present in Soil 2 as observed from the micrographs. Moreover, it should be expected that at higher effective confining stresses, the incremental change in G_{max} would be higher for Soil 2 and its sieved derivatives compared with the other soils.

As regards, the negative power coefficient m of void ratio, e was lowest for Soil 1 followed by Soil 1C, Soil 2, Soil 2B, Soil 1A, Soil 1B and Soil 2A respectively. The variation of coefficient, m can be better assessed when the soils are considered as two separate groups, with one being Soil 1 and its derivative soils and the other one being Soil 2 and its sieved soils. Looking at the two groups independently, it can be observed that for all cases (except Soil 1B), the more crushable the material (higher n), the less significantly void ratio (lower absolute value of m) affects the G_{max} value. This may be explained from the premise that as the more crushable soils are broken down, the void spaces are further filled up, creating a denser material.

4.4.4 Influence of imogolite

Imogolite may also contribute to enhancing the shear stiffness of the soils. From Wells *et al.* (1980) and Wells and Theng (1985) works, it is known that imogolite confers additional rigidity (highly bonded fabric structure) to the soil. Micrographs in Figures 7(a-2), 7(a-3) and 7(e-2) revealed that fibrous webs of imogolite linking allophane are more extensive in Soil 1. Thus the contribution of imogolite to the small strain stiffness might be greater in Soil 1.

It should be highlighted that imogolite is considered as a non-thixotropic material (Wells *et al.*, 1980). Hence, the contribution of imogolite would be limited to low effective confining pressures and distortion of the fibres would also reduce their positive effects. The imogolite webs in Soil 1C were partially affected in some sections because of the sieving process (Figure 7(d-2)). Thus, the imogolites are expected to make a minor contribution to the small stiffness of Soil 1C. As for Soil 2B, imogolites possibly do not have any bearing on the shear stiffness as they transformed to a flaky material after drying.

4.5 Prediction models

According to Gazetas (1991) empirical formulae for small strain shear modulus could be helpful in the following cases:

- for initial design estimations, before carrying out laboratory or site investigations
- for final design calculations in projects where the costs of performing site investigations may be prohibitive
- as a check vis-à-vis values determined by site investigations or by laboratory experiments

Based on the same reasoning, some predictive models have been proposed in the literature. The researchers usually correlated the small-strain shear modulus with the mean effective confining pressure and the void ratio (Hardin & Richart, 1963; Iwasaki & Tatsuoka, 1977; Kokusho *et al.*, 1982; Shibuya & Tanaka, 1996; Shibuya *et al.*, 1997; Wichtmann & Triantafyllidis, 2009; Yang & Gu, 2013, Yang & Liu, 2016, Liu *et al.*, 2016).

The prediction model usually follows the general form:

$$G_{\max} = AF(e)\left[\frac{\sigma\prime}{P_a}\right]^n \qquad (4)$$

where *F(e)* is the void ratio function, σ' is the mean effective stress, P_a is the atmospheric pressure used as a reference for normalization purposes and *A* and *n* are constants.

Mitchell and Soga (2005) and Bui *et al.* (2010) indicated that A could be referred to as a material constant related to the soil properties and fabric. Bui *et al.* (2010) added that there are no unique expression of *F(e)* that could be applied to all soils over a wide range of void ratios. Various forms of *F(e)* have been proposed for different void ratio ranges and for different types of soils. Basically, the void ratio functions could be classified into two groups: hyperbolic functions and exponential functions.
Some of these empirical relationships and their fitting coefficients are summarized in Table 4. As can be seen in this table, there is a large variation in the values of fitting parameters A and n and void ratio function *F(e)* in the literature.

Wichtmann and Triantafyllidis (2009) and Liu *et al.* (2016) studied sandy and granular volcanic soils respectively. They related parameters A and n to the to the grain size distribution through the coefficient of uniformity, U_c. As was the case of Iwasaki and Tatsuoka (1977) who studied sandy soils, Wichtmann and Triantafyllidis (2009) and Liu *et al.* (2016) observed for their materials that the G_{max} values decreased with U_c. This trend could not be confirmed in this research (Figures 15(a-d)) for the kuroboku soils. Albeit, it might be said that at all effective confining stresses (50-200 kPa), the G_{max} value of the soils in their natural states followed the pattern in that G_{max} ought to decrease with increasing U_c (Soil 1, $U_c = 8.034$ and Soil 2, $U_c = 9.216$). The G_{max} of the sieved soils displayed an irregular pattern with U_c. As was mentioned at section 4.2, the use of grain size distribution may be problematic for kuroboku soils. Therefore, in this research, indices from the grain size distribution were not related to the constants A and n. Further studies on natural allophanic soils sampled from a larger number of sites may give a better perspective on the applicability of these indices to this type of soil.

In this study, one exponential function and two hyperbolic functions were considered as void ratio functions. All the prediction models generally produced satisfying results, with R^2 values being greater than 0.90. The

proposed predictive models may be helpful for preliminary design calculations before any in-situ or laboratory measurements are made.

Using an exponential expression for the void ratio function, the following relationship was obtained (R^2 = 0.91):

$$G_{max} = 60.8(e)^{-1.82}\left[\frac{\sigma\prime}{P_a}\right]^{0.56} \quad (5)$$

Using a hyperbolical expression for the void ratio function, the following relationship was obtained (R^2 = 0.91):

$$G_{max} = 268.8\frac{1}{(1+e)^{2.50}}\left[\frac{\sigma\prime}{P_a}\right]^{0.55} \quad (6)$$

Another hyperbolic expression for the void ratio function was tried and the results are shown in Figure 17. The correlation between the measured and predicted results improved (R^2 = 0.97) and the relationship was as follows:

$$G_{max} = 1376.6\frac{(e)^2}{(1+e)^{5.26}}\left[\frac{\sigma\prime}{P_a}\right]^{0.55} \quad (7)$$

In all the above relationships, the G_{max} evaluated is in MPa and P_a was taken as 100kPa. Consideration in future of the effects of ageing would further improve the prediction models.

4.6 Situating the G_{max} of kuroboku soil

Figure 18 shows the variations of small strain shear modulus, G_{max} with void ratio for kuroboku compared with other soils in the literature at an effective confining stress of 100kPa. Kokusho *et al.* (1982) carried out tests on an alluvial normally consolidated clay (Teganuma, alluvial clay). Shibuya and Tanaka (1996) proposed an empirical relation to predict the small strain shear modulus of five clays from Japan (Ariake, Hachirougata, Izumo, Kurihama and Higashi-Ohgishima) and two clays from Europe (Bothkennar (UK) and Fucino (Italy)). Shibuya *et al.* (1997) extended their previous work by including in-situ seismic results from clays St Alban and Drammen and bender element test results on six reconstituted natural clays and two commercially available clays.

Vardanega and Bolton (2012) proposed a similar equation as Shibuya *et al.* (1997) based on several clays (e.g. Bangkok, London and Pisa clays), some silty clays (Windsor, Wallaceburg, Sarnia and Port Stanley), two clayey silts (Hamilton and Chatham) and bay mud. Empirical relationships on several volcanic soils from different locations in Japan as well as New Zealand and Hong Kong were also added. This comprised the works of Miura *et al.* (2003), Sahaphol and Miura (2005), Liu *et al.* (2016), Asadi *et al.* (2020) and

Okewale and Grobler (2020). The equations proposed by Senetakis *et al.* (2012) for crushed rhyolitic volcanic glassy rock was also included, although the country of origin of the material is unknown. Relations for Toyoura sand and Quiou carbonate sand courtesy of the works of Asadi *et al.* (2020) and Lo Presti *et al.* (1997) respectively were included for a better perspective of the small strain shear modulus of different materials.

By plotting equation (7) from section 4.5, it could be deduced that the small strain shear modulus of kuroboku is very comparable to normally consolidated clays. This could be due to the fact that volcanic ash containing allophane or halloysite minerals have probably not experienced overburden stresses greater than their current state (Wesley, 1990; Moon *et al.*, 2017).

A single relation (50-200kPa) can reasonably capture the evolution of G_{max} of the kuroboku soil and the other volcanic soils except for Touhoro, Shirasu, fine-medium and coarse decomposed volcanic rocks. This relation can take the following form ($R^2 = 0.97$):

$$G_{max} = 45.4(e)^{-1.55}\left[\frac{\sigma\prime}{P_a}\right]^{0.58} \quad (8)$$

Note that there can be other volcanic soils within the same void ratio range as kuroboku with more silt size particles or heavier minerals. Thus, these volcanic soils would have higher G_{max} values than kuroboku. However, the present work can only give further impetus to other researchers to collect more data about other volcanic soils and extend the applicability of this general equation.

Touhoro (D_{50} = 5.10mm), Shirasu, fine-medium and coarse decomposed volcanic rocks have all been described as either susceptible to particle breakage or being very crushable (Sahaphol & Miura, 2005; Hyodo *et al.*, 2022; Okewale & Grobler, 2020). The G_{max} of Shirasu, fine-medium and coarse decomposed volcanic soils were in the same range as that of the crushable Quiou carbonate sand. Lo Presti *et al.* (1997) suggested that the crushing of the soils may lead to an increase in contact area or number of contacts and thus a higher shear modulus.

From Figure 18, it can be observed that Mori soil has a very high small strain shear stiffness similar to Toyoura sand. The G_{max} of kuroboku soil is much lower than that of Mori soil. However, in Figure 11, the cyclic strength of Mori soil (which lies within the shaded zone drawn to represent the results of Miura *et al.* (2003)) is lower than that of the kuroboku soil and the allophanic volcanic ash tested by Verdugo (2008). The G_{max} of the latter is in the same range as the kuroboku soil. Hence, usage of shear wave velocity for this type of soil, for assessing liquefaction susceptibility may be doubtful as V_s does not capture other

characteristics like the electrostatic bonding prevalent between the particles which largely explains the liquefaction resistance of allophanic soils.

From the very limited information available in the literature, some data about the dynamic properties of volcanic ash in other parts of the world was gathered (Table 5). We also included the data of volcanic ash soil from Tauranga, New Zealand based on which Chiaro *et al.* (2018) carried out the modelling of the Takanodai landslide in Kumamoto. From the geological information available from Manaaki Whenua - Landcare Research New Zealand Limited (2022), the general nature of the said volcanic ash at Wakite Road, Tauranga, New Zealand is described as being "orthic pumice", although just off the area in the southerly direction "orthic allophanic soils" are also present. Since the exact sampling locations of the soils were not mentioned by Meyer *et al.* (2005), it cannot be confirmed with certainty that the said soils were indeed allophanic.

In general the shear velocities of the kuroboku soil appear slightly less than the volcanic ashes from New Zealand, Colombia and Chile. This would translate into a slightly lower G_{max} value for the kuroboku soil compared to the other soils. The main reason for this observation is believed to be the higher water content owing to the higher allophane content of the kuroboku soil. Furthermore, the specific gravity of the kuroboku soil is smaller than the other volcanic ashes. The presence of heavier minerals or less porous particles may also be another contributing factor. Further in-depth collaborative studies amongst researchers from various parts of the world would undoubtedly complement the current knowledge about the dynamic properties of allophanic soils.

5. Conclusions

The influence of the clay minerals allophane and imogolite on the engineering properties of soils seems underappreciated. It was found that in relation to the 2016 Kumamoto Earthquake, no soil engineering publications referred to the clay mineral imogolite and rare were those papers mentioning about allophane. Furthermore, systematic research on the small strain shear stiffness of allophanic volcanic ash soils is extremely limited. This research set out to address these two points.
A series of index properties, engineering properties, electron microscopy examinations (SEM and FE-SEM) and bender element tests was performed on remoulded kuroboku sampled from two sites located in central Kyushu. The main results and findings are summarized as follows.

(a) Kuroboku is characterised by unusually high natural water (>150%) and fines content (>90%). The kuroboku soil falls in the same category of residual soils which have both "free water" and "water of

crystallization". Simultaneous tests carried out on kuroboku samples at 110°C and lower temperatures revealed that the "water of crystallization" at 50°C was about 20%.

(b) The major soil constituents were the clay minerals allophane and imogolite, together with volcanic glass. Being of aggregate nature, the contact relations are likely to be dominated by face to face interaction. Mesopores (2-50nm) were easily recognizable between allophane domains, between imogolite threads and within diatoms.

(c) Together, the allophane domains and imogolite fibres may occasionally depict a structure similar to an inverted micelle. The presence of imogolite between allophane domains supports the claims of some researchers in that imogolite formation follows that of allophane. Drying led to the dehydration of the imogolite fibres in Soil 2B. However, the allophane domains retained a general stiffness, although in general, there was a visible contraction in their volumes.

(d) The pH in H_2O of the soils tested were about 5. Hence, with strong electrostatic bonds flocculating tendencies would prevail such that in field conditions the soils would exist as aggregated particles. Dispersal of the flocculated particles would provide a better estimation of the clay fraction. However, at the same time the usefulness and applicability of indices like D_{10} if determined from dispersed samples would be doubtful.

(e) Liquefaction was not widespread considering the magnitude of the 2016 Kumamoto Earthquake. Historical spots where liquefaction had occurred and sand boiling locations during the 2016 Kumamoto Earthquake fell mostly outside the zones covered by allophanic soils. The allophanic soils display resistance to sonication and have high cyclic shear resistance. For the evaluation of the susceptibility to liquefaction, instead of grain size distribution, it would be better to consider the stratification of the non-liquefiable allophanic soils with other liquefiable soils.

(f) At the same effective confining pressure, the difference in small strain shear stiffness between all the soils was slight. The myriad of the types of soil components and the contact relation influences the small strain shear stiffness. Presence of isolated, unclothed and larger volcanic shards creates a fragmented and slightly weaker microfabric than the more continuous assemblage network. Diatoms because of their roughness and interlocking contribute to additional shear stiffness at low effective confining pressures. Presence of larger intra-elemental pores for Soil 2 (as observed from the micrographs), also showed up as higher stress exponents values for effective confining stress, confirming the weaker and more crushable nature of the material.

(g) The prediction models for estimating the shear modulus of kuroboku soil generally produced satisfying results ($R^2 = 0.91$ and 0.97). A general equation that can capture the G_{max} of several volcanic soils and the kuroboku soil was also proposed. Based on previous works carried out by other researchers, it could be deduced that the small strain shear modulus of kuroboku is very comparable to normally consolidated clays and smaller than that of more granular volcanic soils. From a cursory assessment, it also seemed that the shear wave velocity of the kuroboku soils is slightly less compared to volcanic ash soils in New Zealand, Colombia and Chile.

CRediT authorship contribution statement

M. Gobin: Conceptualization, Methodology, Validation, Formal analysis, Investigation, Data Curation, Visualization, Writing – original draft, Writing – review & editing. **N. Yasufuku**: Resources, Supervision, Project administration. **G. Liu**: Methodology, Investigation, Supervision. **M. Watanabe**: Methodology, Investigation, Resources, Supervision. **R. Ishikura**: Supervision.

Declaration of Competing Interest

The authors declare that they have no known competing financial interests or personal relationships that could have appeared to influence the work reported in this paper.

Acknowledgments

The first author is indebted to the Japanese Government (Monbukagakusho: MEXT) for sponsoring his studies. The first author wishes to express his gratitude to Professor Kiyonobu Kasama for his suggestions during the former's progress examinations. The authors also thank Dr. Muneharu Kudou for taking the pain to sample the soils from Oita prefecture during the COVID pandemic. The support of Kyushu University Library for procuring research materials and the help of Mr. Michio Nakashima, technical staff are also acknowledged.

References

Allbrook, R.F., 1985. The effect of allophane on soil properties. *Applied clay science*, *1*(1-2), pp.65-69.

Asadi, M. B., Asadi, M. S., Orense, R. P., & Pender, M. J., 2020. Small-Strain Stiffness of Natural Pumiceous Sand. *Journal of Geotechnical and Geoenvironmental Engineering*, *146*(6), 06020006.

Bennett, R. H., and Hulbert, M. H. 1986. *Clay Microstructure*. International Human Resources Development Corporation, Boston/ Houston/London.

Bishop, J.L. and Rampe, E.B., 2016. Evidence for a changing Martian climate from the mineralogy at Mawrth Vallis. *Earth and Planetary Science Letters*, *448*, pp.42-48.

BMKG and JICA, 2018. BMKG and JICA, 2018: Palu Earthquake strong motion wave form by observation system developed by Japan. [Online]. Available from: https://committees.jsce.or.jp/eec205/system/files/%E3%83%91%E3%83%AB%E5%9C%B0%E9%9C%87%E5%BC%B7%E9%9C%87%E6%B3%A2%E5%BD%A2%E8%A8%98%E9%8C%B2%E9%80%9F%E5%A0%B11022_0.pdf [Accessed 19th February 2022].

Bui, M. T., Clayton, C. R. I. and Priest, J. A., 2010. The universal void ratio function for small strain shear modulus. *International Conferences on Recent Advances in Geotechnical Earthquake Engineering and Soil Dynamics*, p. Paper 29.

Cabinet Office of Government of Japan, 2016. Estimated Economic Impact Due to the 2016 Kumamoto Earthquakes (in Japanese). [Online]. Available from: http://www5.cao.go.jp/keizai3/kumamotoshisan/kumamotoshisan20160523.pdf [Accessed February 12th, 2022].

Chen, H. and Lee, C.F., 2004. Geohazards of slope mass movement and its prevention in Hong Kong. *Engineering Geology*, *76*(1-2), pp.3-25.

Chiaro, G., Alexander, G., Brabhaharan, P., Massey, C., Koseki, J., Yamada, S. and Aoyagi, Y., 2017. Reconnissance report on geotechnical and geological aspects of the 14-16 April 2016 Kumamoto earthquakes, Japan. *Bulletin of the New Zealand Society for Earthquake Engineering*, 50(3), pp. 365–393.

Chiaro, G., Chew, K. S. Y. and Kim, J., 2018a. Numerical analyses of the earthquake-induced Takanodai landslide , Kumamoto , Japan.

Chiaro, G., Umar, M., Kiyota, T., & Massey, C., 2018b. The Takanodai landslide, Kumamoto, Japan: insights from post-earthquake field observations, laboratory tests, and numerical analyses. In *Geotechnical Earthquake Engineering and Soil Dynamics V: Slope Stability and Landslides,*

Laboratory Testing, and In Situ Testing (pp. 98-111). Reston, VA: American Society of Civil Engineers.

Chitravel, S., Otsubo, M. and Kuwano, R., 2022. Effects of internal erosion on the cyclic and post-cyclic mechanical behaviours of reconstituted volcanic ash. *Soils and Foundations*, *62*(2), p.101111.

Choo, H., Bate, B. and Burns, S.E., 2015. Effects of organic matter on stiffness of overconsolidated state and anisotropy of engineered organoclays at small strain. *Engineering Geology*, *184*, pp.19-28.

Clayton, C. R. I., 2011. Stiffness at small strain: Research and practice. *Geotechnique*, 61(1), pp. 5–37.

Collins, K.T. and McGown, A., 1974. The form and function of microfabric features in a variety of natural soils. *Geotechnique*, *24*(2), pp.223-254.

Cunningham, M.J., Lowe, D.J., Wyatt, J.B., Moon, V.G. and Churchman, G.J., 2016. Discovery of halloysite books in altered silicic Quaternary tephras, northern New Zealand. *Clay Minerals*, *51*(3), pp.351-372.

Dao, L.Q., Cui, Y.J., Tang, A.M., Pereira, J.M., Li, X.L. and Sillen, X., 2015. Impact of excavation damage on the thermo-hydro-mechanical properties of natural Boom Clay. *Engineering Geology*, *195*, pp.196-205.

Day, R.W., 1995. Engineering properties of diatomaceous fill. *Journal of geotechnical engineering*, *121*(12), pp.908-910.

Doi, I., Kamai, T., Azuma, R. and Wang, G., 2019. A landslide induced by the 2016 Kumamoto Earthquake adjacent to tectonic displacement-generation mechanism and long-term monitoring. *Engineering Geology*, *248*, pp.80-88.

Earthquake Research Committee, Headquarters for Earthquake Research Promotion (2013) Long-term evaluation of the Futagawa and Hinagu fault zones (2013 revision). 66 (in Japanese). [Online]. Available from:
http://www.jishin.go.jp/main/chousa/13feb_chi_kyushu/k_11.pdf.
[Accessed 02th December 2021]

Eswaran, H., 1972. Morphology of allophane, imogolite and halloysite. *Clay minerals*, *9*(3), 281-285.

Ferrari, A., Eichenberger, J. and Laloui, L., 2013. Hydromechanical behaviour of a volcanic ash. *Géotechnique*, *63*(16), pp.1433-1446.

Ferreira, C., da Fonseca, A. and Santos, J. A., 2007. Comparison of Simultaneous Bender Elements and Resonant. *Soil Stress-Strain Behavior: Measurement, Modeling and Analysis. Solid Mechanics and Its Applications*, pp. 523–535.

Fiantis, D., Ginting, F. I., Nelson, M., & Minasny, B., 2019. Volcanic ash, Insecurity for the people but securing fertile soil for the future. *Sustainability*, *11*(11), 3072.

Fieldes, M., 1955. Clay mineralogy of New Zealand soils, Part II: Allophane and related mineral colloids. *New Zealand Journal of Science and Technology*, *37*(3), pp.336-350.

Fiorillo, F. and Wilson, R.C., 2004. Rainfall induced debris flows in pyroclastic deposits, Campania (southern Italy). *Engineering Geology*, *75*(3-4), pp.263-289.

Fourie, A.B., Irfan, T.Y., Carvalho, J.D., Simmons, J.V. and Wesley, L.D., 2012. Microstructure, mineralogy and classification of residual soils. In Blight, G.E. and Leong, E.C. (ed*.). Mechanics of residual soils*. Boca Raton: CRC Press, pp. 41-61.

Frattini, P., Crosta, G.B., Fusi, N. and Dal Negro, P., 2004. Shallow landslides in pyroclastic soils: a distributed modelling approach for hazard assessment. *Engineering Geology*, *73*(3-4), pp.277-295.

Gazetas, G., 1991. Foundation vibrations. In H. Y. Fang (ed.). *Foundation engineering handbook*. NY: Springer New York, (pp. 553-593).

Geospatial Information Authority of Japan, 2016. *[Geographical Survey Institute] Fault around Kawayo, Minamiaso Village (photographed on April 18, 2016)*. 18 April. [Online Video]. Available from: https://www.youtube.com/watch?v=bS6ftodIHeI
[Accessed March 24th, 2022].

Geospatial Information Authority of Japan, 2022a. GSI Map. (in Japanese). [Online]. Available from: https://maps.gsi.go.jp/
[Accessed January 07th, 2022].

Geospatial Information Authority of Japan, 2022b. Explanation of active fault map (active fault map of urban area) (in Japanese). [Online]. Available from: https://www.gsi.go.jp/bousaichiri/guidebook.html

[Accessed February 13th, 2022].

Giang, P. H. H., Van Impe, P. O., Van Impe, W. F., Menge, P., & Haegeman, W., 2017. Small-strain shear modulus of calcareous sand and its dependence on particle characteristics and gradation. *Soil Dynamics and Earthquake Engineering*, *100*, 371-379.

Gibbons, W., Moreno, T., & Kojima, T., 2016. Field geotraverse, geoparks and geomuseums. In: Moreno, T., Wallis, S., Kojima, T., Gibbons, W. (ed.) *The Geology of Japan*. London: The Geological Society, pp. 485-508.

Goldsmith, P.R. and Smith, E.H., 1985. Tunnelling soils in South Auckland, New Zealand. *Engineering geology*, *22*(1), pp.1-11.

Gu, X., Yang, J., Huang, M., & Gao, G., 2015. Bender element tests in dry and saturated sand: Signal interpretation and result comparison. *Soils and Foundations*. Elsevier, 55(5), pp. 951–962.

Hardin, B. O., and Richart, Jr., F. E. 1963. Elastic wave velocities in granular soils, *Journal of the Soil Mechanics and Foundations Division,* ASCE, Vol. 89, No. SM1, pp. 33–65.

Harsh, J., Chorover, J. and Nizeyimana, E., 2002. Allophane and imogolite. In: Dixon, J.B. and Schulze, D.G. (ed.) *Soil Mineralogy with environmental applications*, *7*. United States - Madison, Wisconsin.: Soil Science Society of America Inc., pp.291-322.

Hazarika, H., Kokusho, T., Kayen, R.E., Dashti, S., Fukuoka, H., Ishizawa, T., Kochi, Y., Matsumoto, D., Furuichi, H., Hirose, T. and Fujishiro, T., 2017. Geotechnical damage due to the 2016 Kumamoto Earthquake and future challenges. *Lowland Technology International*, *19*(3, Dec), pp.203-218.

Head, K. H., 1992. *Manual of Soil Laboratory Testing. Volume 1: Soil Classification of Compaction Tests*. London, Pentech Press.

Henmi, T. and Wada, K., 1976. Morphology and composition of allophane. *American Mineralogist*, *61*(5-6), pp.379-390.

Hernandez, O., Cordão Neto, M.P. and Caicedo, B., 2018. Structural features and hydro-mechanical behaviour of a compacted andesitic volcanic soil. *Géotechnique Letters*, *8*(3), pp.195-200.

Herrera, M.C., Lizcano, A. and Santamarina, J.C., 2007. Colombian volcanic ash soils. *Characterization and engineering properties of natural soils*, pp.2385-2409.

Hyodo, T., Wu, Y. and Hyodo, M., 2022. Influence of fines on the monotonic and cyclic shear behaviour of volcanic soil "Shirasu". *Engineering Geology*, *301*, p.106591.

Ikeda, M., Toda, S., Kobayashi, S., Ohno, Y., Nishizaka, N. and Ohno, I., 2009. Tectonic model and fault segmentation of the Median Tectonic Line active fault system on Shikoku, Japan. *Tectonics*, *28*(5).

Ishihara, K., 1985. Stability of natural deposits during earthquakes. *Proc. of 11th ICSMFE, 1985*, *1*, 321-376.

Ishihara, K., 1996. Soil behaviour in earthquake geotechnics. Oxford Science Publications.

Iwasaki, T., & Tatsuoka, F., 1977. Effects of grain size and grading on dynamic shear moduli of sands. *Soils and foundations*, *17*(3), 19-35.

Iyoda, F., Hayashi, S., Arakawa, S., John, B., Okamoto, M., Hayashi, H. and Yuan, G., 2012. Synthesis and adsorption characteristics of hollow spherical allophane nano-particles. *Applied Clay Science*, *56*, pp.77-83.

Jacquet, D., 1990. Sensitivity to remoulding of some volcanic ash soils in New Zealand. *Engineering Geology*, *28*(1-2), pp.1-25.

Japan Meteorological Agency, 2022a. *Climate of the Kyushu (North) district*. [Online]. Available from: https://www.data.jma.go.jp/gmd/cpd/longfcst/en/tourist/file/Northern_Kyushu.html#:~:text=Kyushu%20(North)%20has%20one%20of,%2C%20to%20Kyushu%20(North).
[Accessed 06th February 2022].

Japan Meteorological Agency, 2022b. *Tables of Monthly Climate*. [Online]. Available from: https://www.data.jma.go.jp/obd/stats/data/en/smp/index.html
[Accessed 06th February 2022].

Japan National Committee on Earthquake Engineering, (n.d). Niigata Earthquake of 1964. [Online]. Available from:
https://www.iitk.ac.in/nicee/wcee/article/vol3_S-78.pdf
[Accessed March 24th, 2022].

Japanese Geotechnical Society Standards, 2009. JGS 0051: Method of classification of geomaterials for engineering purposes. Tokyo: The Japanese Geotechnical Society.

Japanese Geotechnical Society Standards, 2009. JGS 0141: Test method for liquid limit and plastic limit of soils. Tokyo: The Japanese Geotechnical Society.

Kaiser, A., Holden, C., Beavan, J., Beetham, D., Benites, R., Celentano, A., Collett, D., Cousins, J., Cubrinovski, M., Dellow, G. and Denys, P., 2012. The Mw 6.2 Christchurch earthquake of February 2011: preliminary report. *New Zealand journal of geology and geophysics*, *55*(1), pp.67-90.

Karube, J., Nakaishi, K., Sugimoto, H. and Fujihira, M., 1996. Size and shape of allophane particles in dispersed aqueous systems. *Clays and clay minerals*, *44*(4), pp.485-491.

Kayen, R.E., Dashti, S., Kokusho, T., Hazarika, H., Franke, K., Oettle, N.K., Wham, B., Calderon, J.R., Briggs, D., Guillies, S. and Cheng, K., 2017. *Geotechnical aspects of the 2016 MW 6.2, MW 6.0, and MW 7.0 Kumamoto earthquakes*. Geotechnical Extreme Events Reconnaissance Association.

Kayen, R., Kokusho, T., Hazarika, H., Dashti, S., Calderon, J.R., Franke, T.K., Oettle, N.K., Wham, B., Louis-Kayen, G.P., Sitar, R. and Louis-Kayen, N.M., 2018. Geotechnical extreme-event reconnaissance (GEER) investigation to the 2016 Mw6. 0, Mw6. 2and Mw7. 0 Kumamoto Japan Earthquakes. *Lowland Technology International*, *19*(4, March), pp.267-274.

Kitazono, Y., Suzuki, A., Kajiwara, M., & Aramaki, S., 1985. Effect of Undrained Preloading on Compacted Allophenic-Volcanic Ash Soils. *材料*, *34*(377), 221-227 (in Japanese).

Kitazono, Y., Suzuki, A., Kajiwara, M., & Aramaki, S., 1987. Contribution of micro structure to repeated loading effect on compacted allophaneous volcanic ash soil. *Soils and Foundations*, *27*(4), 23-33.

Kiyota, T., Ikeda, T., Konagai, K. and Shiga, M., 2017. Geotechnical damage caused by the 2016 Kumamoto earthquake, Japan. *International Journal of Geoengineering Case Histories*, *4*(2), pp.78-95.

Kokusho, T., Yoshida, Y., & Esashi, Y., 1982. Dynamic properties of soft clay for wide strain range. *Soils and Foundations*, *22*(4), 1-18.

Kubotera, H., Kusaba, T. and Shishibe, I., 2013. Distribution and horizons sequence of non-allophanic Kuroboku Soil in Kuju Plateau, Kyushu, Japan. *Pedologist* (in Japanese).

Kuribayashi, E. and Tatsuoka, F., 1975. Brief review of liquefaction during earthquakes in Japan. *Soils and Foundations*, *15*(4), pp.81-92.

Kusumoto, S., 2016. Structural Analysis of Calderas by Semiautomatic Interpretation of the Gravity Gradient Tensor: A Case Study in Central Kyushu, Japan. In: Nemeth, K. (ed.). *Updates in Volcanology: From Volcano Modelling to Volcano Geology*. Croatia: InTech, pp. 105-140.

Lawrence, F.V. 1963. Propagation of ultrasonic waves through sand. Massachusetts Institute of Technology, Cambridge, Mass. Research Report R63–08

Le, T.M.H., Eiksund, G.R., Strøm, P.J. and Saue, M., 2014. Geological and geotechnical characterisation for offshore wind turbine foundations: A case study of the Sheringham Shoal wind farm. *Engineering Geology*, *177*, pp.40-53.

Leamy, M. L., 1984. International Committee on the Classification of Andisols (ICOMAND) Circular letter No. 6. *New Zealand Soil Bureau, DSIR, Lower Hutt*.

Levard, C., Doelsch, E., Basile-Doelsch, I., Abidin, Z., Miche, H., Masion, A., Rose, J., Borschneck, D. and Bottero, J.Y., 2012. Structure and distribution of allophanes, imogolite and proto-imogolite in volcanic soils. *Geoderma*, *183*, pp.100-108.

Liu, X., Yang, J., Wang, G., & Chen, L., 2016. Small-strain shear modulus of volcanic granular soil: An experimental investigation. *Soil Dynamics and Earthquake Engineering*. Elsevier, 86, pp. 15–24.

Liu, G., 2019. *Evaluation of liquefaction potential in relation to the shearing history using shear wave velocity* (Doctoral dissertation, Kyushu University).

Liu, X., Zhang, N. and Lan, H., 2019. Effects of sand and water contents on the small-strain shear modulus of loess. *Engineering Geology*, *260*, 105202.

Lo Presti, D.C.F., Jamiolkowski, M., Pallara, O., Cavallaro, A. and Pedroni, S., 1997. Shear modulus and damping of soils. *Géotechnique*, *47*(3), pp.603-617.

Lowe, D.J. and Palmer, D.J. （2005）: Andisols of New Zealand and Australia. *Journal of Integrated Field Science, 2*, 39-65.

Maeda, T., Takenaka, H. and Warkentin, B.P., 1977. Physical properties of allophane soils. In *Advances in Agronomy* (Vol. 29, pp. 229-264). Academic Press.

Manaaki Whenua - Landcare Research New Zealand Limited, 2022. *New Zealand Soil Classification.* [Online]. Available from:

https://soils-maps.landcareresearch.co.nz/
[Accessed 26th February 2022].

Martínez, R.C., Silva-Yumi, J., Serrano, C.M. and Lescano, G.C., 2021. Allophane, A Natural Nanoparticle Present In Andisoles Of Ecuador, Properties And Applications. *La Granja. Revista de Ciencias de la Vida*, *33*(1), pp.53-66.

Matsuda, T., 1981. Active faults and damaging earthquakes in Japan—macroseismic zoning and precaution fault zones. *Earthquake prediction: An international review*, *4*, pp.279-289.

McDaniel, P.A., Lowe, D.J., Arnalds, O., Ping, C.-L., 2012. Andisols. In: Huang, P.M., Li, Y., Sumner, M.E. (ed.) *Handbook of Soil Sciences*, 2nd edition. Vol. 1: Properties and Processes. Boca Raton, FL: CRC Press, pp. 33.29- 33.48.

Menendez, O.H., Lopes, B.D.C.F.L., Caicedo, B. and Neto, M.P.C., 2022. Microscopic and mineralogical characteristics behind the engineering properties of a compacted andesitic volcanic soil. *Journal of South American Earth Sciences*, *115*, p.103752.

Meyer, V., Larkin, T., & Pender, M., 2005. The shear strength and dynamic shear stiffness of some New Zealand volcanic ash soils. *Soils and foundations*, *45*(3), 9-20.

Mitchell, J. K., & Soga, K., 2005. *Fundamentals of soil behavior*. 3rd edition. New York: John Wiley & Sons.

Miura, S., Yagi, K. and Asonuma, T., 2003. Deformation-strength evaluation of crushable volcanic soils by laboratory and in-situ testing. *Soils and Foundations*, *43*(4), pp.47-57.

Miyazaki, K., Ozaki, M., Saito, M., & Toshimitsu, S., 2016. The kyushu–ryukyu arc. In: Moreno, T., Wallis, S., Kojima, T., Gibbons, W. (ed.) *The Geology of Japan*. London: The Geological Society, pp. 139-174.

Mizota, C., Carrasco, M.A. and Wada, K., 1982. Clay mineralogy and some chemical properties of Ap horizons of Ando soils used for paddy rice in Japan. *Geoderma*, *27*(3), pp.225-237.

Moon, V.G., Lowe, D.J., Cunningham, M.J., Wyatt, J., Churchman, G.J., de Lange, W.P., Mörz, T., Kreiter, S., Kluger, M.O., Jorat, M.E. and Rotonda, T., 2015. Sensitive pyroclastic-derived halloysitic soils in northern New Zealand: interplay of microstructure, minerals, and geomechanics. In *Volcanic*

Rocks and Soils. Proceedings of the International Workshop on Volcanic Rocks and Soils, Lacco Ameno, Ischia Island, Italy (pp. 3-21). Taylor & Francis, London, UK.

Moon, V., 2016. Halloysite behaving badly: geomechanics and slope behaviour of halloysite-rich soils. *Clay minerals*, *51*(3), pp.517-528.

Moon, V.G., Mills, P.R., Kluger, M.O., Lowe, D.J., Churchman, G.J., de Lange, W.P., Hepp, D.A., Kreiter, S. and Mörz, T., 2017. Sensitive pyroclastic soils in the Bay of Plenty, New Zealand: microstructure to failure mechanisms. In *20th New Zealand Geotechnical Society Symposium NZGS2017* (pp. 1-8). New Zealand Geotechnical Society.

Mukunoki, T., K. Kasama, S. Murakami, H. Ikemi, R. Ishikura, T. Fujikawa, N. Yasufuku, and Y. Kitazono, 2016. Reconnaissance report on geotechnical damage caused by an earthquake with JMA seismic intensity 7 twice in 28 h, Kumamoto, Japan. *Soils and Foundations*. Elsevier, 56(6), pp. 947–964.

Nakada, S., Yamamoto, T., & Maeno, F., 2016. Miocene–Holocene volcanism. In: Moreno, T., Wallis, S., Kojima, T., Gibbons, W. (ed.) *The Geology of Japan*. London: The Geological Society, pp. 273-308.

Nakagawa, T. and Ishiguro, M., 1994. Hydraulic conductivity of an allophanic Andisol as affected by solution pH. *Journal of environmental quality*, *23*(1), pp.208-210.

National Agriculture and Food Research Organization (2022). Japan soil inventory (in Japanese). [Online]. Available from:
https://soil-inventory.rad.naro.go.jp/
[Accessed 04th January 2022].

National Research Institute for Earth Science and Disaster Resilience, 2022. Strong-motion seismograph networks (K-NET, KiK-net). [Online]. Available from:
https://www.kyoshin.bosai.go.jp/
[Accessed 15th March 2022].

Niazi, M., Mortgat, C. P., & Schneider, J. F., 1992. Attenuation of peak ground acceleration in central California from observations of the 17 October, 1989 Loma Prieta earthquake. Earthquake engineering & structural dynamics, 21(6), 493-507.

Nishimura, S., 2006. *Laboratory study on anisotropy of natural London Clay* (Doctoral dissertation,

Imperial College London (University of London)).

Ola, S.A., 1980. Mineralogical properties of some Nigerian residual soils in relation with building problems. *Engineering geology*, *15*(1-2), pp.1-13.

Ogo, K., Hazarika, H., Kokusho, T., Matsumoto, D., Ishibashi, S. and Sumartini, W.O., 2018. Analysis of liquefaction of volcanic soil during the 2016 Kumamoto Earthquake based on boring data. *Lowland Technology International*, *19*(4, March), pp.245-250.

Okewale, I.A. and Coop, M.R., 2017. A study of the effects of weathering on soils derived from decomposed volcanic rocks. *Engineering Geology*, *222*, pp.53-71.

Okewale, I.A. and Grobler, H., 2020. A study of dynamic shear modulus and breakage of decomposed volcanic soils. *J GeoEng*, *15*(1), pp.53-66.

Ono, K., 1963. The Geological Sheet Map of Japan 'Kuju' with explanatory text, 1:50,000. Geological Survey of Japan.

Ono, K. and Watanabe, K., 1985. Geological Map of Aso Volcano, 1:50,000. Geological Survey of Japan.

Orense, R.P., Zapanta, A., Hata, A. and Towhata, I., 2006. Geotechnical characteristics of volcanic soils taken from recent eruptions. *Geotechnical & Geological Engineering*, *24*(1), pp.129-161.

Otowa, M., 1986. Morphology and classification. In: Wada, K. (ed.) *Ando soils in Japan*. Fukuoka, Japan: Kyushu University Press, pp 3-20.

Pan, K., Yuan, Z.H., Zhao, C.F., Tong, J.H. and Yang, Z.X., 2022. Undrained shear and stiffness degradation of intact marine clay under monotonic and cyclic loading. *Engineering Geology*, *297*, p.106502.

Pérez, N.A., Bucio, L., Lima, E., Soto, E. and Cedillo, C., 2016. Identification of allophane and other semi-crystalline and amorphous phases on pre-Hispanic Mexican adobe earth bricks from Cholula, Mexico. *Microchemical Journal*, *126*, pp.349-358.

Rao, S.M., 1995. Mechanistic approach to the shear strength behaviour of allophanic soils. *Engineering Geology*, *40*(3-4), pp.215-221.

Rao, S.M., 1996. Role of apparent cohesion in the stability of Dominician allophane soil slopes. *Engineering Geology*, *43*(4), pp.265-279.

Reading, A.J., 1991. Stability of tropical residual soils from Dominica, West Indies. *Engineering Geology*, *31*(1), pp.27-44.

Rendón, M.I., Viviescas, J.C., Osorio, J.P. and Hernández, M.S., 2020. Chemical, mineralogical and geotechnical index properties characterization of volcanic ash soils. *Geotechnical and Geological Engineering*, *38*(3), pp.3231-3244.

Rocchi, I., Coop, M.R. and Maccarini, M., 2017. The effects of weathering on the physical and mechanical properties of igneous and metamorphic saprolites. *Engineering Geology*, *231*, pp.56-67.

Rouse, W. C., Reading, A. J. and Walsh, R. P. D., 1986. Volcanic soil properties in dominica, west indies. *Engineering Geology*, 23(1), pp. 1–28.

Rouse, C., 1990. The mechanics of small tropical flowslides in Dominica, West Indies. *Engineering Geology*, *29*(3), pp.227-239.

Sahaphol, T. and Miura, S., 2005. Shear moduli of volcanic soils. *Soil Dynamics and Earthquake Engineering*, 25(2), pp. 157–165.

Santamarina, J.C., Klein, K.A. and Fam, M.A., 2001. *Soils and waves*. New York: J. Wiley & Sons.

Schnaid, F., & Huat, B. B. K., 2013. Sampling and testing of tropical residual soils. In: Huat, B.B., Toll, D.G. and Prasad, A. (ed.) *Handbook of tropical residual soils engineering*. Boca Raton: CRC Press, pp. 65-112.

Senetakis, K., Anastasiadis, A. and Pitilakis, K., 2012. The small-strain shear modulus and damping ratio of quartz and volcanic sands. *Geotechnical Testing Journal*, 35(6).

Shibata, T., Oka, F. and Ozawa, Y., 1996. Characteristics of ground deformation due to liquefaction. *Soils and foundations*, *36*, pp.65-79.

Shibuya, S., & Tanaka, H., 1996. Estimate of elastic shear modulus in Holocene soil deposits. *Soils and foundations*, *36*(4), 45-55.

Shibuya, S., Hwang, S. C., & Mitachi, T., 1997. Elastic shear modulus of soft clays from shear wave velocity measurement. *Geotechnique*, *47*(3), 593-601.

Shirahama, Y., Yoshimi, M., Awata, Y., Maruyama, T., Azuma, T., Miyashita, Y., Mori, H., Imanishi, K., Takeda, N., Ochi, T. and Otsubo, M., 2016. Characteristics of the surface ruptures associated with

the 2016 Kumamoto earthquake sequence, central Kyushu, Japan. *Earth, Planets and Space*, *68*(1), pp.1-12.

Shirley, D. J., & Hampton, L. D., 1978. Shear-wave measurements in laboratory sediments. *The Journal of the Acoustical Society of America*, *63*(2), 607-613.

Sieffermann, G. and Millot, G., 1969. Equatorial and tropical weathering of recent basalts from Cameroon: allophanes, halloysite, metahalloysite, kaolinite and gibbsite. In *Proc. Int. Clay Conf., Tokio, Japan* (Vol. 1, pp. 417-430).

Simas, F.N., Schaefer, C.E.G., Melo, V.F., Guerra, M.B., Saunders, M. and Gilkes, R.J., 2006. Clay-sized minerals in permafrost-affected soils (Cryosols) from King George Island, Antarctica. *Clays and clay minerals*, *54*(6), pp.721-736.

Smalley, I.J., Ross, C.W. and Whitton, J.S., 1980. Clays from New Zealand support the inactive particle theory of soil sensitivity. *Nature*, *288*(5791), pp.576-577.

Song, K.C. and Yoo, S.H., 1994. Andic Properties of Major Soils in Cheju Island-III. Conditions for Formation of Allophane. *Korean Journal of Soil Science and Fertilizer*, *27*(3), pp.149-157 (In Korean).

Song, B., Tsinaris, A., Anastasiadis, A., Pitilakis, K., & Chen, W., 2017. Small-strain stiffness and damping of Lanzhou loess. *Soil Dynamics and Earthquake Engineering*, *95*, 96-105.

Sorem, R.K., 1982. Volcanic ash clusters: tephra rafts and scavengers. *Journal of Volcanology and Geothermal Research*, *13*(1-2), pp.63-71.

Sudo, T., 1978. An outline of clays and clay minerals in Japan. In: Sudo, T. and Shimoda, S. (ed.) *Clays and clay minerals of Japan*. Tokyo: Kodansha Ltd., pp. 1-103

Suzuki, Y., 2017. *1: 25,000 Active fault map "Aso" commentary* (in Japanese). [Online]. Available from: https://www.gsi.go.jp/common/000193621.pdf
[Accessed February 12th, 2022].

Takahashi, T., & Shoji, S., 2002. Distribution and classification of volcanic ash soils. *Global Environmental Research-English Edition-*, *6*(2), 83-98.

Takashima, R., Kuwabara, S., Sato, T., Takemura, K., & Nishi, H., 2017. Utility of trace elements in apatite for discrimination and correlation of Quaternary ignimbrites and co-ignimbrite ashes, Japan. *Quaternary Geochronology*, *41*, 151-162.

Tamura, K., Miura, H., Kaneko, S., Sano, T. and Kubotera, H., 2021. Soil-forming factors. In *The Soils of Japan* (pp. 13-51). Springer, Singapore.

Tanaka, K., 1992. Slope hazards and clay minerals. *Journal of the Clay Science Society of Japan (in Japanese)*, *32*(1), pp.16-22.

Terzaghi, K., 1958. Design and performance of Sasumua dam. Proc. Instn. Civ. Engrs., UK., 9,369–394.

Tsukamoto, Y., Ishihara, K. and Kamata, T., 2009. Undrained shear strength of soils under flow deformation. *Géotechnique*, *59*(5), pp.483-486.

The Overseas Coastal Area Development Institute of Japan, 2009. *Technical Standards and Commentaries for Port and Harbour Facilities in Japan*, pp. 282–287.

Ugolini, F.C., Dahlgren, R., LaManna, J., Nuhn, W. and Zachara, J., 1991. Mineralogy and weathering processes in recent and Holocene tephra deposits of the Pacific Northwest, USA. *Geoderma*, *51*(1-4), pp.277-299.

van Ballegooy, S., Green, R.A., Lees, J., Wentz, F. and Maurer, B.W., 2015. Assessment of various CPT based liquefaction severity index frameworks relative to the Ishihara (1985) H1–H2 boundary curves. *Soil Dynamics and Earthquake Engineering*, *79*, pp.347-364.

Vardanega, P. J., & Bolton, M. D., 2013. Stiffness of clays and silts: Normalizing shear modulus and shear strain. *Journal of Geotechnical and Geoenvironmental Engineering*, *139*(9), 1575-1589.

Verdugo, R., 2008. Singularities of geotechnical properties of complex soils in seismic regions. *Journal of geotechnical and geoenvironmental engineering*, *134*(7), pp.982-991.

Viggiani, G. and Atkinson, J. H., 1995. Stiffness of fine-grained soil at very small strains. *Geotechnique*, 45(2), pp. 249–265.

Wada, K., Yoshinaga, N., Yotsumoto, H., Ibe, K. and Aida, S., 1970. High resolution electron micrographs of imogolite. *Clay Minerals*, *8*(4), pp.487-489.

Wada, K., Henmi, T., Yoshinaga, N.T. and Patterson, S.H., 1972. Imogolite and allophane formed in saprolite of basalt on Maui, Hawaii. *Clays and Clay Minerals*, *20*(6), pp.375-380.

Wada, K., 1978. Allophane and imogolite. In: Sudo, T. and Shimoda, S. (ed.) *Clays and clay minerals of Japan*. Tokyo: Kodansha Ltd., pp. 147-187.

Wada, K., 1985. The distinctive properties of Andosols. In: Stewart, B.A (ed.) *Advances in soil science*. Springer New York, Vol.2, NY, pp. 173-229.

Wada, K., eds., 1986. *Ando soils in Japan*. Kyushu University Press, Fukuoka, Japan.

Wada, K. 1989. Allophane and imogolite. In: J. B. Dixon and S. B. Weed (ed.) *Minerals in soil environments*. 2nd edition. Madison, WI: SSSA Book Ser. 1. SSSA, pp. 1051–1087.

Wada, K., Arnalds, O., Kakuto, Y., Wilding, L.P. and Hallmark, C.T., 1992. Clay minerals of four soils formed in eolian and tephra materials in Iceland. *Geoderma*, *52*(3-4), pp.351-365.

Wakamatsu, K., Senna, S., & Ozawa, K., 2017a. Liquefaction and its Characteristics during the 2016 Kumamoto Earthquake. Proceedings of the Japan Earthquake Engineering Society, 17 (4), pp.4_81-4_100 (in Japanese).

Wakamatsu, K., Senna, S., & Ozawa, K., 2017b. Liquefaction during the Kumamoto Earthquakes on April 14 and 16, 2016. *Lowland Technology International*, *19*(3, Dec), 191-202.

Wallace, K.B., 1973. Structural behaviour of residual soils of the continually wet Highlands of Papua New Guinea. *Geotechnique*, *23*(2), pp.203-218.

Watabe, Y. and Nishimura, S., 2020. Ground movements and damage in Satozuka district, Sapporo due to 2018 Hokkaido Eastern Iburi Earthquake. *Soils and Foundations*, *60*(5), pp.1331-1356.

Webb, J.A. and Finlayson, B.L., 1984. Allophane and opal speleothems from granite caves in south-east Queensland. *Journal of the Geological Society of Australia*, *31*(3), pp.341-349.

Wells, N., Theng, B.K.G. and Walker, G.D., 1980. Behaviour of imogolite gels under shear. *Clay Science*, *5*(5), pp.257-265.

Wells, N. and Theng, B.K., 1985. Factors affecting the flow behavior of soil allophane suspensions under low shear rates. *Journal of colloid and interface science*, *104*(2), pp.398-408.

Wesley, L.D., 1973. Some basic engineering properties of halloysite and allophane clays in Java, Indonesia. *Geotechnique*, *23*(4), pp.471-494.

Wesley, L.D., 1990. Influence of structure and composition on residual soils. *Journal of geotechnical engineering*, *116*(4), pp.589-603.

Wesley, L. D., 2010. *Geotechnical engineering in residual soils*. John Wiley & Sons.

Wichtmann, T. and Triantafyllidis, T., 2009. Influence of the grain-size distribution curve of quartz sand on the small strain shear modulus Gmax. *Journal of Geotechnical and Geoenvironmental Engineering*, 135(10), pp. 1404–1418.

Yamashita, S., Kawaguchi, T., Nakata, Y., Mikami, T., Fujiwara, T., & Shibuya, S., 2009. Interpretation of international parallel test on the measurement of G max using bender elements. *Soils and Foundations*, 49(4), pp. 631–650.

Yang, J. and Gu, X. Q., 2013. Shear stiffness of granular material at small strains: Does it depend on grain size? *Geotechnique*, 63(2), pp. 165–179.

Yang, J. and Liu, X., 2016. Shear wave velocity and stiffness of sand: The role of non-plastic fines. *Geotechnique*, 66(6), pp. 500–514.

Yasuda, S., & Tohno, I., 1988. Sites of reliquefaction caused by the 1983 Nihonkai-Chubu earthquake. *Soils and Foundations*, *28*(2), 61-72.

Yasuda, S., Yoshida, Y., Kobayashi, T., & Mizunaga, T., 1999. Slope failures triggered by an earthquake and a heavy rain in Chiba. In *Slope stability engineering* (pp. 539-544).

Yasuhara, K., Komine, H., Murakami, S., Chen, G., Mitani, Y., & Duc, D. M., 2012. Effects of climate change on geo-disasters in coastal zones and their adaptation. *Geotextiles and Geomembranes*, *30*, 24-34.

Ying, Z., Cui, Y.J., Benahmed, N. and Duc, M., 2021. Changes of small strain shear modulus and microstructure for a lime-treated silt subjected to wetting-drying cycles. *Engineering Geology*, *293*, p.106334.

Yoshinaga, N., & Aomine, S., 1962. Imogolite in some Ando soils. *Soil Science and Plant Nutrition*, *8*(3), 22-29.

Yoshinaga, N., 1986. Mineralogical characteristics – II Clay Minerals. In: Wada, K. (ed.) *Ando soils in Japan*. Fukuoka, Japan: Kyushu University Press, pp 41-56.

Youd, T. L., & Garris, C. T., 1995. Liquefaction-induced ground-surface disruption. *Journal of Geotechnical Engineering*, *121*(11), 805-809.

Zhang, G., 2007. Soil nanoparticles and their influence on engineering properties of soils. In *Advances in measurement and modeling of soil behavior* (pp. 1-13).

Zhao, B., 2021. Landslides triggered by the 2018 Mw 7.5 Palu supershear earthquake in Indonesia. *Engineering Geology*, *294*, p.106406.

Highlights

- Allophane domains and imogolite fibres may depict an inverted micelle type morphology
- pH affects electrostatic bonds, which influence the properties of allophanic soils
- Allophanic soils show liquefaction resistance and their stratification is a key point
- Soil components, contact relations and pores determine the small strain shear modulus
- Small strain shear modulus of volcanic ash is similar to normally consolidated clays

Table 1 Index properties of soil tested

Soil	G_s	D_{10} (mm)	D_{50} (mm)	U_c	U_c'
Soil 1	2.172	0.00392	0.0244	8.034	1.264
Soil 1A	2.136	0.00329	0.0173	6.870	1.107
Soil 1B	2.113	0.00280	0.0118	5.394	1.071
Soil 1C	2.258	0.00351	0.0272	10.016	1.214
Soil 2	2.390	0.00406	0.0305	9.216	1.603
Soil 2A	2.302	0.00418	0.0225	6.818	1.243
Soil 2B	2.364	0.0177	0.0489	3.086	1.422

G_s: specific gravity; D_{10}: effective size; D_{50}: mean particle size;

U_c: coefficient of uniformity; U_c': coefficient of gradation

Table 2 Liquid and Plastic limit

Soil	Moisture content, w (%)	Liquid limit, LL (%)	Plastic limit, PL (%)	Plasticity Index, I_P
Soil 1	160	170	144	26
Soil 2	157	183	135	48

Table 3 Comparison of 2016 Kumamoto Earthquake and other earthquakes that induced liquefaction

Earthquake	Maximum seismic intensity (M_w)	Maximum ground acceleration	Reference
Sulawesi (2018)	7.5	EW:281 Gal; NS:203 Gal;UD:335 Gal; compositing of 3 vectors: 400 Gal	BMKG & JICA, 2018 Zhao, 2021
Hokkaido Eastern Iburi (2018)	6.6	EW: 904 Gal; NS: 1004 Gal; UD:1591Gal; compositing of 3 vectors: 1796 Gal	NIED, 2022
Kumamoto (Mainshock – 16 April 2016)	7.0	EW: 1157 Gal; NS: 653 Gal; UD:873 Gal; compositing of 3 vectors: 1362 Gal	NIED, 2022
Kumamoto (Foreshock – 14 April 2016)	6.2	EW: 925 Gal; NS: 760 Gal; UD:1399 Gal; compositing of 3 vectors: 1580 Gal	NIED, 2022
Christchurch (22 February 2011)	6.2	2.2 g (vertical) and 1.7 g (horizontal) near the epicentre and up to 0.8 g (vertical) and 0.7 g (horizontal) in the city centre	Kaiser *et al.*, 2012
Kobe (1995)	6.9	818 Gal	Shibata *et al.*, 1996
Loma Prieta (1989)	7.1	0.64g	Niazi *et al.*, 1992 Youd & Garris, 1995
Nihonkai-Chubu (1983)	7.7	278 Gal	Yasuda & Tohno, 1988
Niigata (1964)	7.5	400 Gal	Japan National Committee on Earthquake Engineering, n.d.

Table 4 Existing coefficients for equation (4) (adapted from Mitchell, J. K. & Soga, K., 2005)

Soil Type		A	$F(e)$	n	Void Ratio Range	Test Method[a]	Reference
Alluvial clay		90	$\frac{(7.32-e)^2}{(1+e)}$	0.6	1.7–3.8	Cyclic TX	Kokusho *et al.* (1982)
Several clays		5,000	$e^{-1.5}$	0.5	1–5	SCPT	Shibuya and Tanaka (1996)
Several clays		24000	$\frac{1}{(1+e)^{2.4}}$	0.5	1–6	SCPT	Shibuya *et al.* (1997)
Carbonate sand (Quiou)		708	$e^{-1.3}$	0.62	0.831-1.281	RC, TS	Lo Presti *et al.* (1997)
Volcanic soil (Shirasu)		10276	$e^{-2.46}$	0.52	1.2-1.5	Cyclic TX	Miura *et al.* (2003)
Volcanic soils	Touhoro	1255	$e^{-0.18}$	0.7	2.9-5.3	BE & Cyclic TX	Sahaphol & Miura (2005)
	Mori	3294	$e^{-1.2}$	0.6	0.6-1.15		
	Kitami	3876	$e^{-1.42}$	0.56	1.2-1.7		
Crushed rhyolitic volcanic rock (V1-V5)		$(-3.04\times U_c+52.02)$ [b]	$e^{-(0.28\times U_c+0.98)}$	0.55	0.794-1.25	RC	Senetakis *et al.* (2012)
Several clays, bay mud, clayey silts & highly plastic silts		20,000	$\frac{1}{(1+e)^{2.4}}$	0.5	0.48–6.15	RC, TS, DSS, BE & Cyclic TX	Vardanega & Bolton (2013)
Volcanic soil -Naganuma		58.32	$\frac{(2.17-e)^2}{(1+e)}$	0.58	0.8–1.05	RC	Liu *et al.* (2016)
Coarse grained completely decomposed volcanic rock	Silt	50.63	$e^{-1.3}$	0.45	1.24-1.58	BE	Okewale and Grobler (2020)
	Fine/medium sand	65.49	$e^{-1.3}$	0.43	1.13-1.54		
	Coarse sand	82.25	$e^{-1.3}$	0.54	1.02-1.26		
Natural pumice (NP) sand	NP1	1300	$e^{-0.88}$	0.72	1.04-1.74	BE	Asadi *et al.* (2020)
	NP2	1091	$e^{-0.64}$	0.74	0.95-1.56		
	NP3	2448	$e^{-1.68}$	0.59	0.65-0.99		
Toyoura		5223	$e^{-1.48}$	0.5	0.61-0.89		

[a] RC: resonant column test, TX: triaxial test, TS: torsional shear test, DSS: direct simple shear, BE: bender element test, SCPT: seismic cone test. [b] U_c: coefficient of uniformity: 1.53 - 4.18.

Table 5 Properties of some volcanic ash in New Zealand, Colombia, Chile and Japan

Country	Nature of ash	Type of sample	Testing method	Dominant clay material	w(%)	G_s	σ' (kPa)	V_s (m/s)	Reference
New Zealand	Rhyolite*[1]	Undisturbed	Torsion test	Not mentioned	59.5-93.5	2.59 - 2.61	37-85*[2]	126-137	Meyer *et al.*, 2005
Colombia	Andesite and dacite	Undisturbed & Remoulded	Bender element	Halloysite	29-119	2.50 - 2.67	*[3]	100-180	Herrera *et al.*, 2007
Chile	Not mentioned	Undisturbed (U) & Remoulded (R)	Bender element	Allophane	78.1-124.2	2.46-2.74*[4]	50-200	160-200 (U) 120-170 (R)	Verdugo, 2008
Japan (this study)	Andesite	Remoulded	Bender element	Allophane	~160*[5]	2.11-2.39	50-200	42-162	

*[1]The nature of the volcanic ash was not mentioned by Meyer *et al.* (2005). However, from the work of Moon *et al.* (2015) on soils in the Tauranga region in New Zealand, we may reasonably deduce that the nature of the ash is of rhyolitic origin.
*[2]The effective confining pressures at which the torsion tests were carried out were not explicitly mentioned by Meyer *et al.* (2005). The values herein mentioned were estimated from the depth from which the samples were taken.
*[3]Herrera *et al.* (2007) tabulated the V_s obtained from their experiments. The corresponding effective confining pressure range was not specified.
*[4]The specific gravity, G_s of the allophanic soils was not mentioned by Verdugo (2008). The G_s values in the table were estimated from the dry densities and initial void ratios.
*[5]The natural water content was adjusted for water of crystallization.

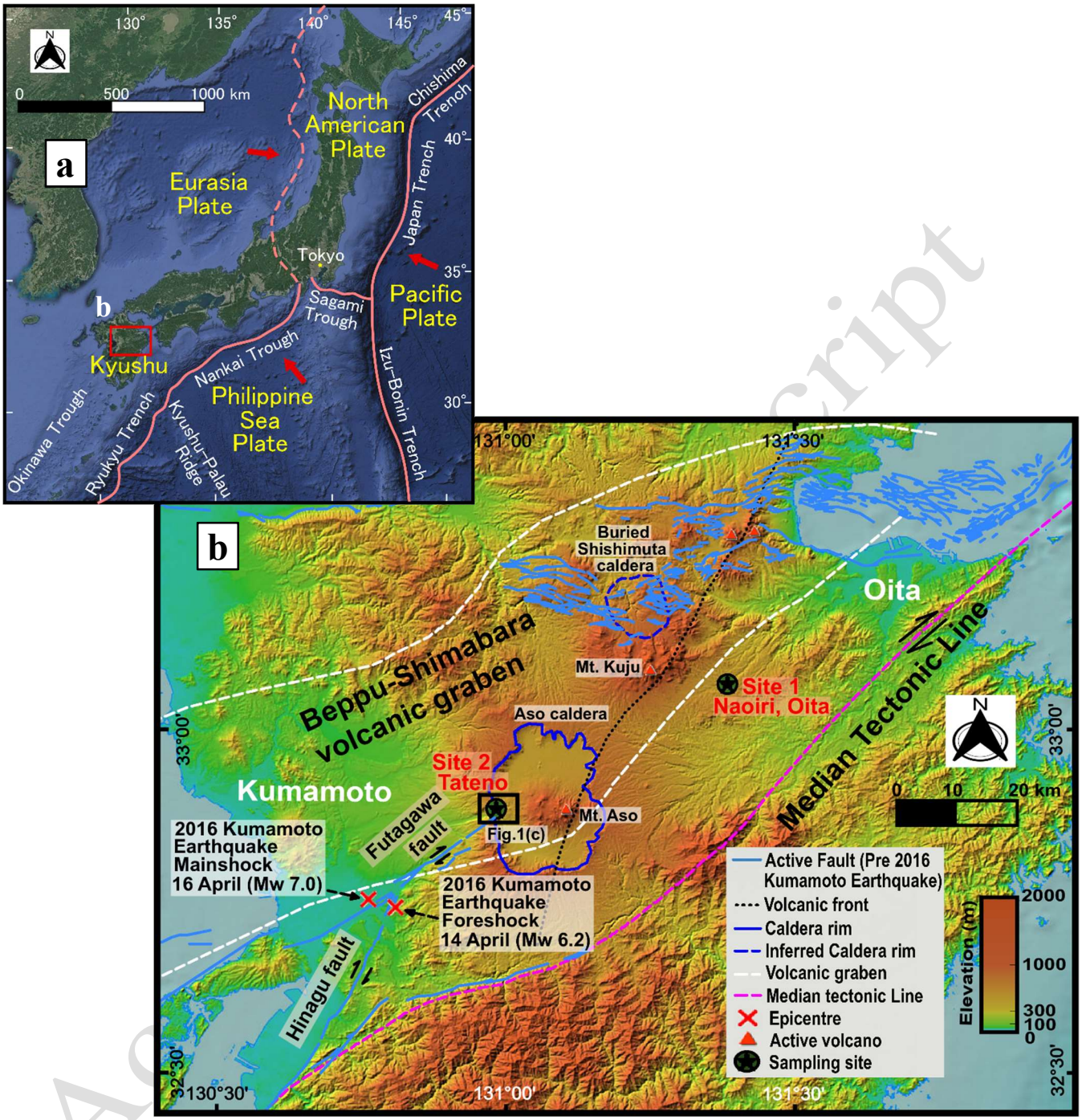

Figure 1 a Location of studied area, in Kyushu Island in the south-western part of Japan (Source map from Google Map). **b** Map of central Kyushu with sampling sites (Source map is the color-coded elevation map created by the Geospatial Information Authority of Japan (2022a). *Light blue lines* are active fault lines which had been recognized prior to the 2016 Kumamoto Earthquake by the Earthquake Research Committee, Headquarters for Earthquake Research Promotion (2013). *Crosses* indicate the epicentres of the foreshock and mainshock events of the earthquake as determined by the Japan Meteorological Agency (Geospatial Information Authority of Japan, 2022a). *Dark blue full lines* denote the Aso caldera. *Dark blue dotted lines* represent the inferred rim of the Shishimuta caldera which was drawn based on Kusumoto (2016). *Red triangles* show the position of active volcanoes according to JMA. *Dotted black line*s represent the volcanic front which has been drawn according to Miyazaki *et al.* (2016). The Beppu-Shimabara volcanic graben and the Median Tectonic Line were sketched according to Gibbons *et al.* (2016).

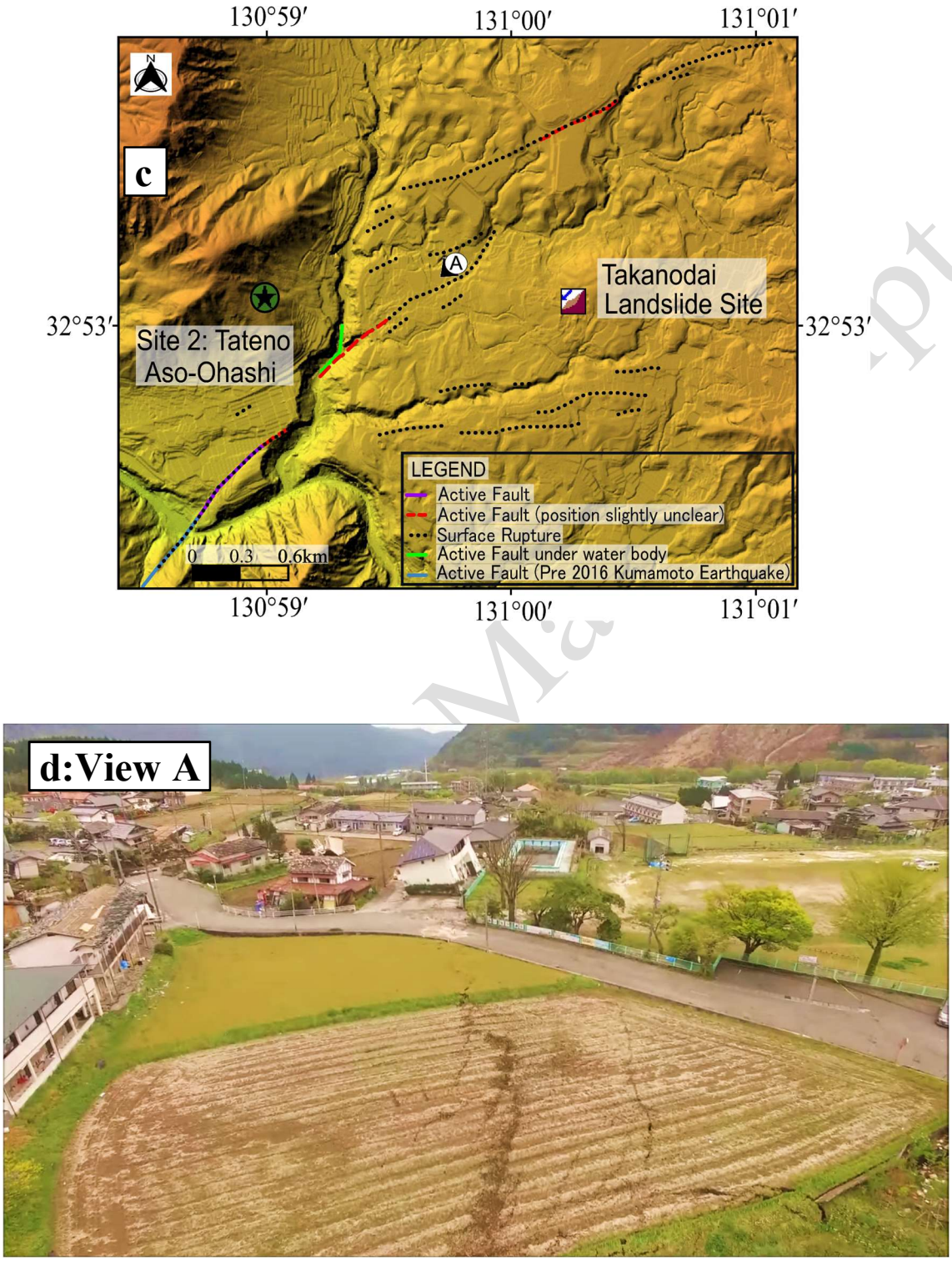

Figure 1 c Magnified image of inset region in **b**. The map was drawn from the information available from Suzuki (2017) and Geospatial Information Authority of Japan (2022a; 2022b). In the aftermath of the Kumamoto Earthquake, it shows the extension of the Futagawa fault in the east north east direction, presence of an active fault under the Kurokawa river at the foot of Site 2 and numerous surface ruptures. **d - View A** shows the photo of the surface rupture in Kawayo, Minami Aso, taken on 18 April 2016 by Geospatial Information Authority of Japan (2016).

Figure 2 (a) Kuroboku sample (Soil 1)

Figure 2 (b) Kuroboku sample (Soil 2)

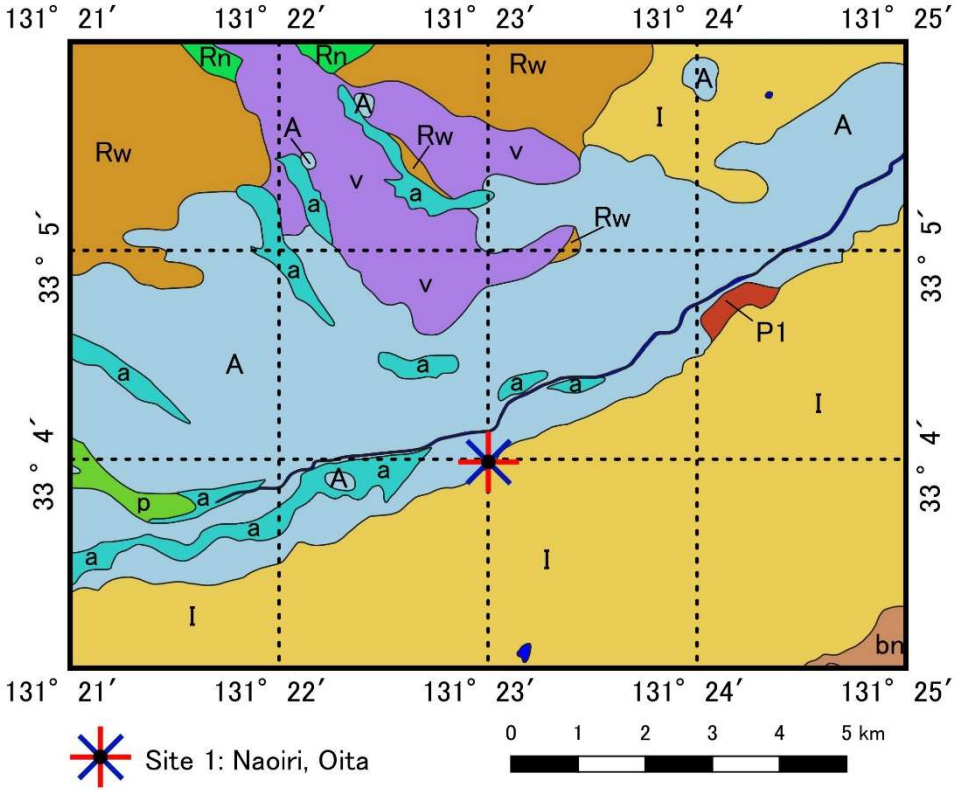

Pleistocene recent

a Gravel, sand and mud (Alluvium)

A Hornblende-bearing pyroxene andesite – welded tuff and pumice tuff-breccia (Serikawa pyroclastic flow – Aso volcano)

v Gravel and sand (Volcanic fan gravel and talus)

Pliocene

I Pyroxene andesite (welded tuff) – Imaichi pyroclastic flow

p Volcanic ash and pumice

P1 Pyroxene andesite (Kakura andesite – Shonai volcanic rocks)

Rn Hornblende-biotite dacite (Nagayu rhyolites – Shonai volcanic rocks)

Rw Hornblende-biotite rhyolite – welded tuff and pumice tuff (Nagayu rhyolites – Shonai volcanic rocks)

Other features

bn Mica schist (Asaji metamorphic rocks)

Water

Figure 3 (a) Geological Map of Site 1, based on Ono (1963), The Geological Sheet Map of Japan 'Kuju' with explanatory text, 1:50,000 (Geological Survey of Japan).

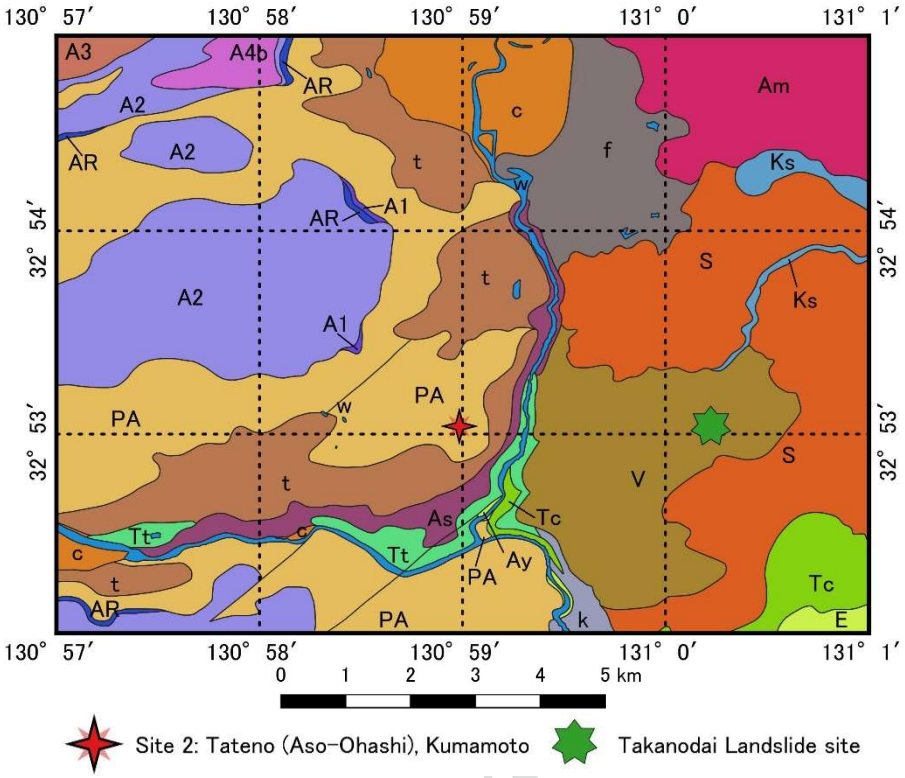

Latest Pleistocene to Holocene

- A1 Augite-hypersthene dacite (Aso-1 Pyroclastic Flow – Welded tuff)
- A2 Hypersthene augite dacite (Aso-2A B Pyroclastic Flow – Welded tuff, in part non-welded deposit of scoria)
- A3 Hypersthene augite dacite (Aso-3 Pyroclastic Flow – Vitric ash, pumice or scoria and welded tuff)
- A4b Pyroxene-hornblende dacite (Aso-4A Pyroclastic Flow – Non-welded deposit of vitric ash and pumice, rich in accidental block)
- Am Augite olivine andesite or olivine augite andesite (Akamizu lava flow)
- AR Hypersthene augite andesite or augite hypersthene andesite (Aso-2R Welded Pyroclastics – Densely welded pyroclastic rock, in part secondary-flowed)
- As Augite olivine andesite or olivine augite andesite (Akase lava flow)
- Ay Augite-olivine basalt (Ayugaerinotaki lava flow)
- c Mud, sand and gravel (Caldera-fill deposit)
- E Hypersthene augite andesite or augite hypersthene andesite (Eboshidake Volcano lava flow and pyroclastic rock)
- f Sand, gravel and silt (Fan deposit)
- k Silt, sand and volcanic ash (Kugino Formation)
- Ks Augite-olivine basalt (Kishimadake Volcano – Lava flow)
- S Augite-hypersthene dacite (Sawatsuno lava flow)
- t Gravel, sand and silt (Talus)
- Tc Hypersthene augite andesite or augite hypersthene andesite (Tochinoki lava flow, with welded pyroclastic rock)
- Tt Augite-hypersthene dacite (Tateno lava flow)
- V Pyroxene-biotite rhyolite (Kusasenrigahama Volcano lava flow)

Late Pliocene - Pleistocene

- PA Pyroxene andesite lava flow and dike

Other features

- w Water

Figure 3 (b) Geological Map of Site 2, based on Ono and Watanabe (1985), Geological Map of Aso Volcano, 1:50,000 (Geological Survey of Japan).

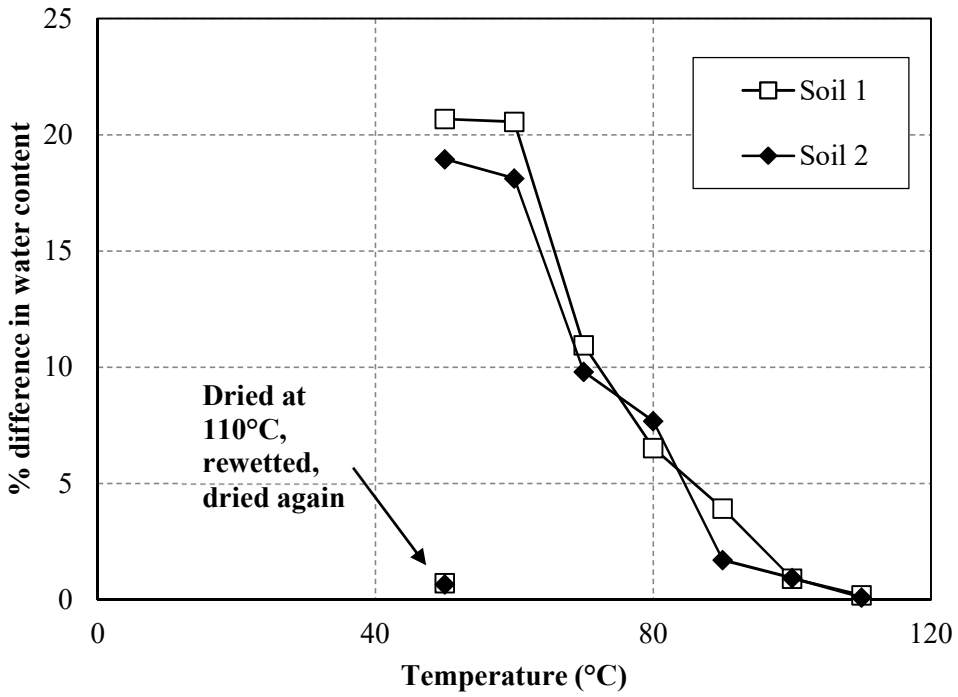

Figure 4 Water content difference for kuroboku at different temperatures compared to 110°C

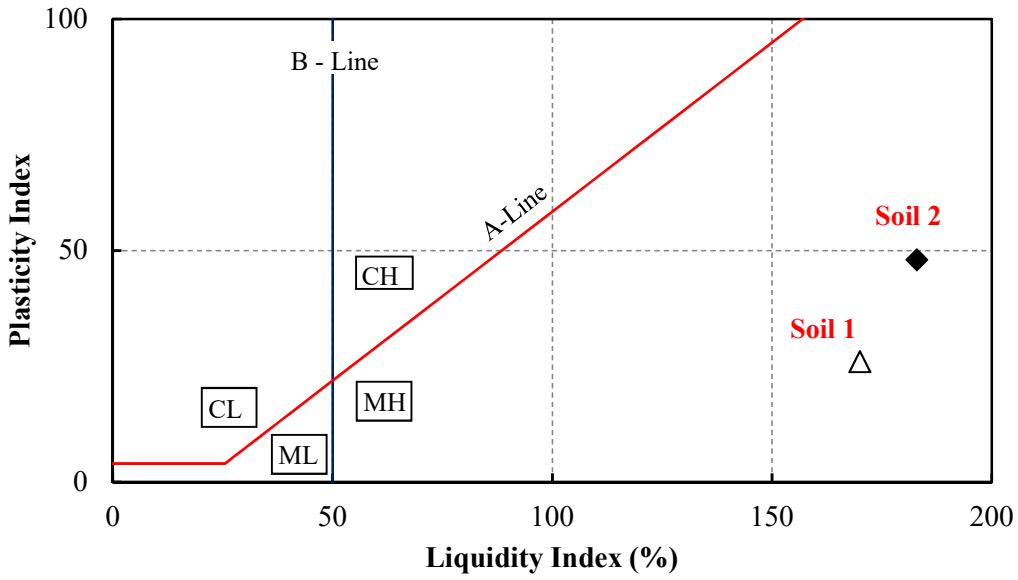

Figure 5 (a) Plasticity chart

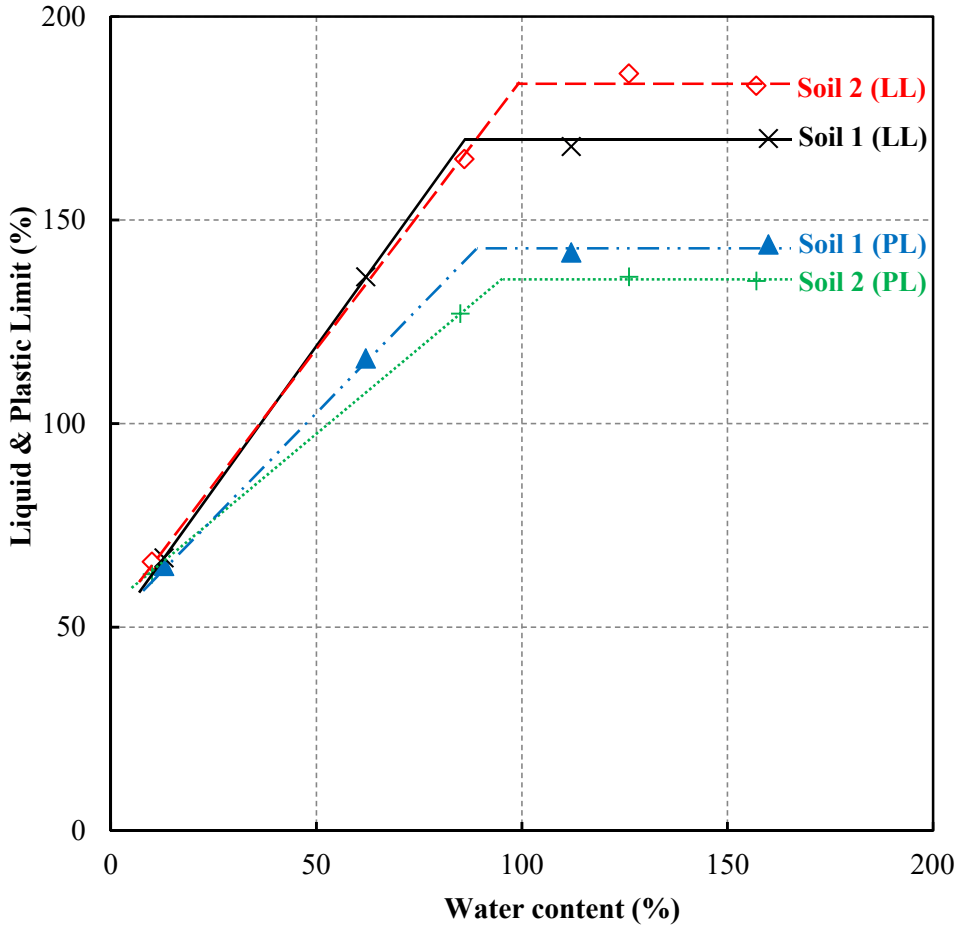

Figure 5 (b) Liquid and Plastic limit variation with water content

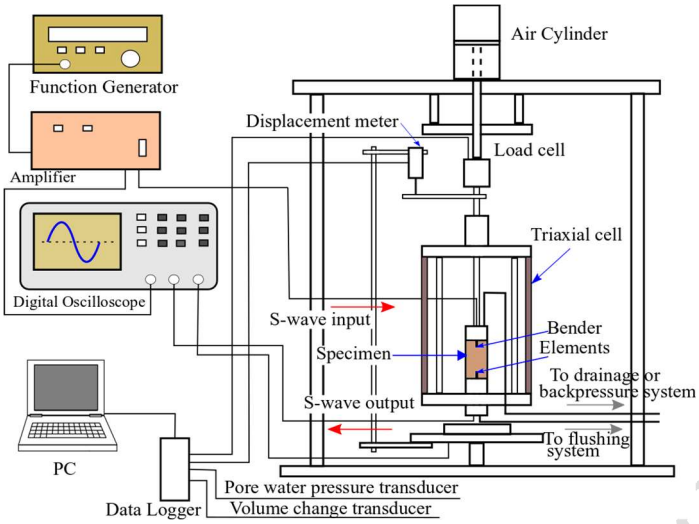

Figure 6 Schematic Diagram of testing device

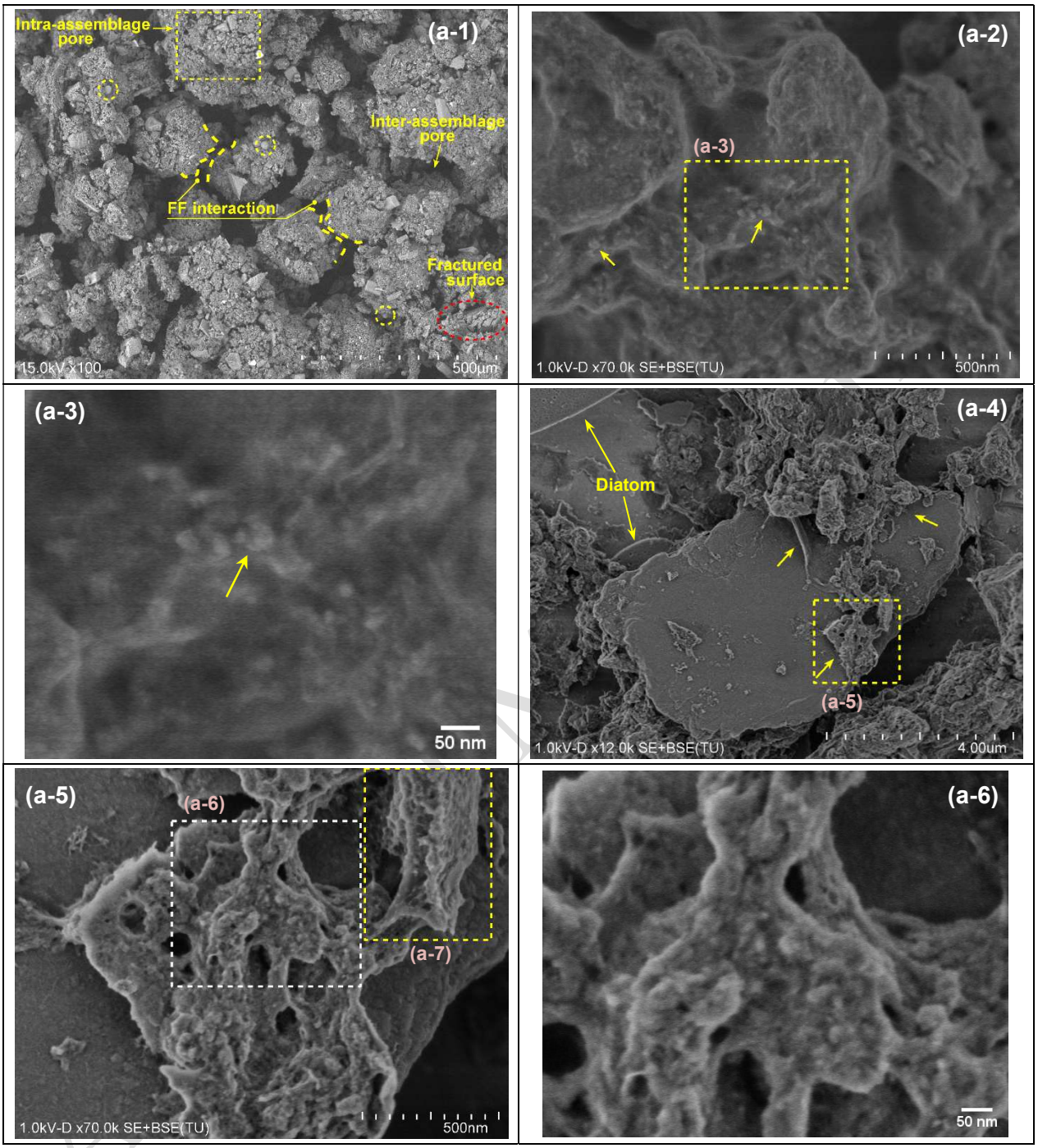

Figure 7 (a-1) SEM image of Soil 1 showing inter and intra assemblage pores, face to face (FF) interaction and fractured volcanic shards. Dotted circles denote occasional spheroidal particles; **(a-2)** FE-SEM image of Soil 1, with arrows indicating allophane spherules aggregations to a domain; **(a-3)** Magnified image of inset region in **(a-2)**; **(a-4)** FE-SEM image of Soil 1 showing diatoms. Arrows indicate that despite sonication, imogolite fibres weaved around the allophane domains and remained attached to a platy-shaped particle; **(a-5)** Magnified image of inset region in **(a-4)**; **(a-6)** Magnified image of inset region in **(a-5)** displaying resistance to sonication of allophane domains and imogolite

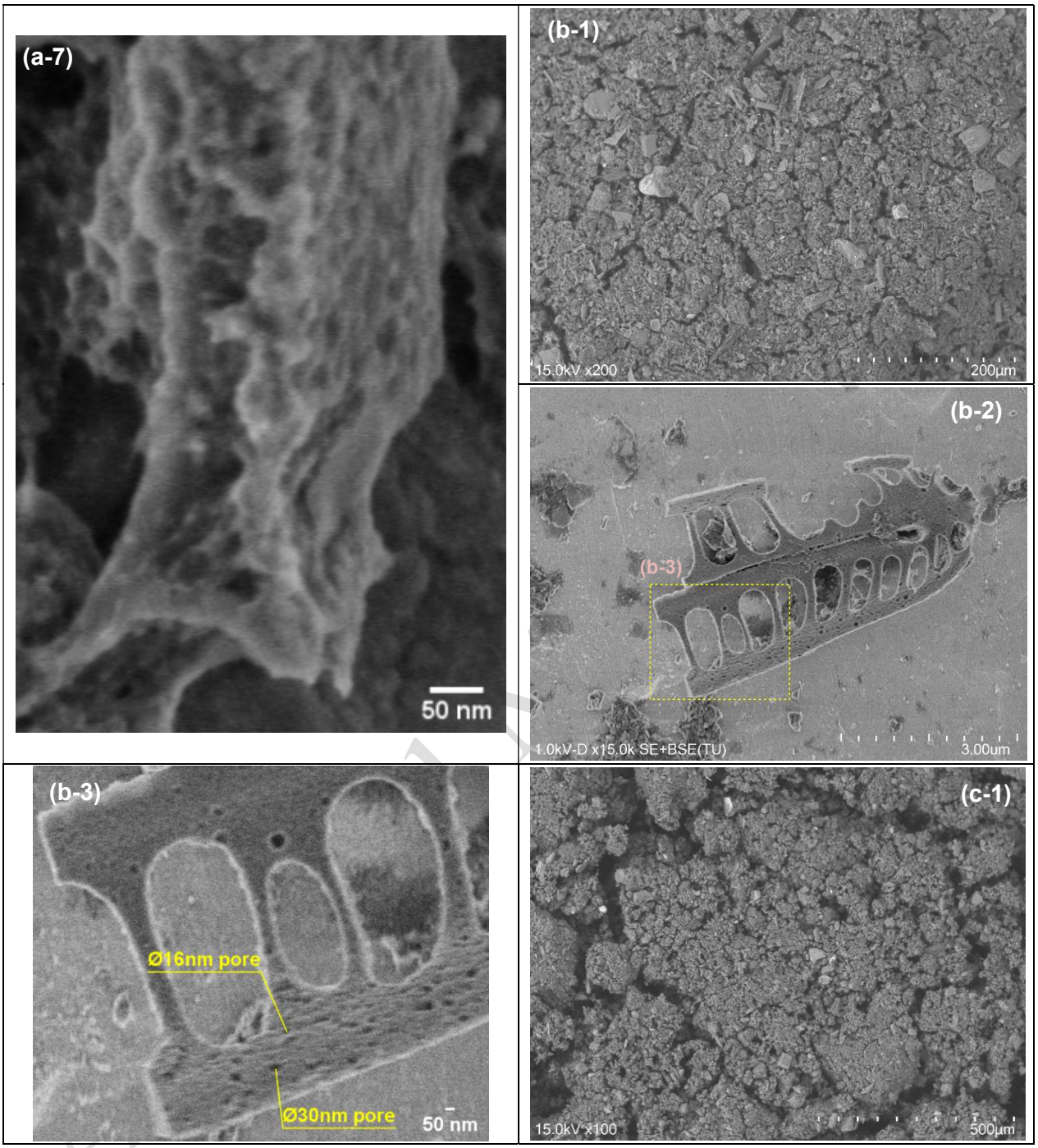

Figure 7 (a-7) Magnified image of inset region in **(a-5)** showing array of allophane domains enveloped by imogolite; **(b-1)** SEM image of Soil 1A; **(b-2)** FE-SEM image of a pennate diatom (in Soil 1A) broken near its central nodule. **(b-3)** Magnified image of inset region in **(b-2)** indicating the rough and porous nature of the diatom; **(c-1)** SEM image of Soil 1B.

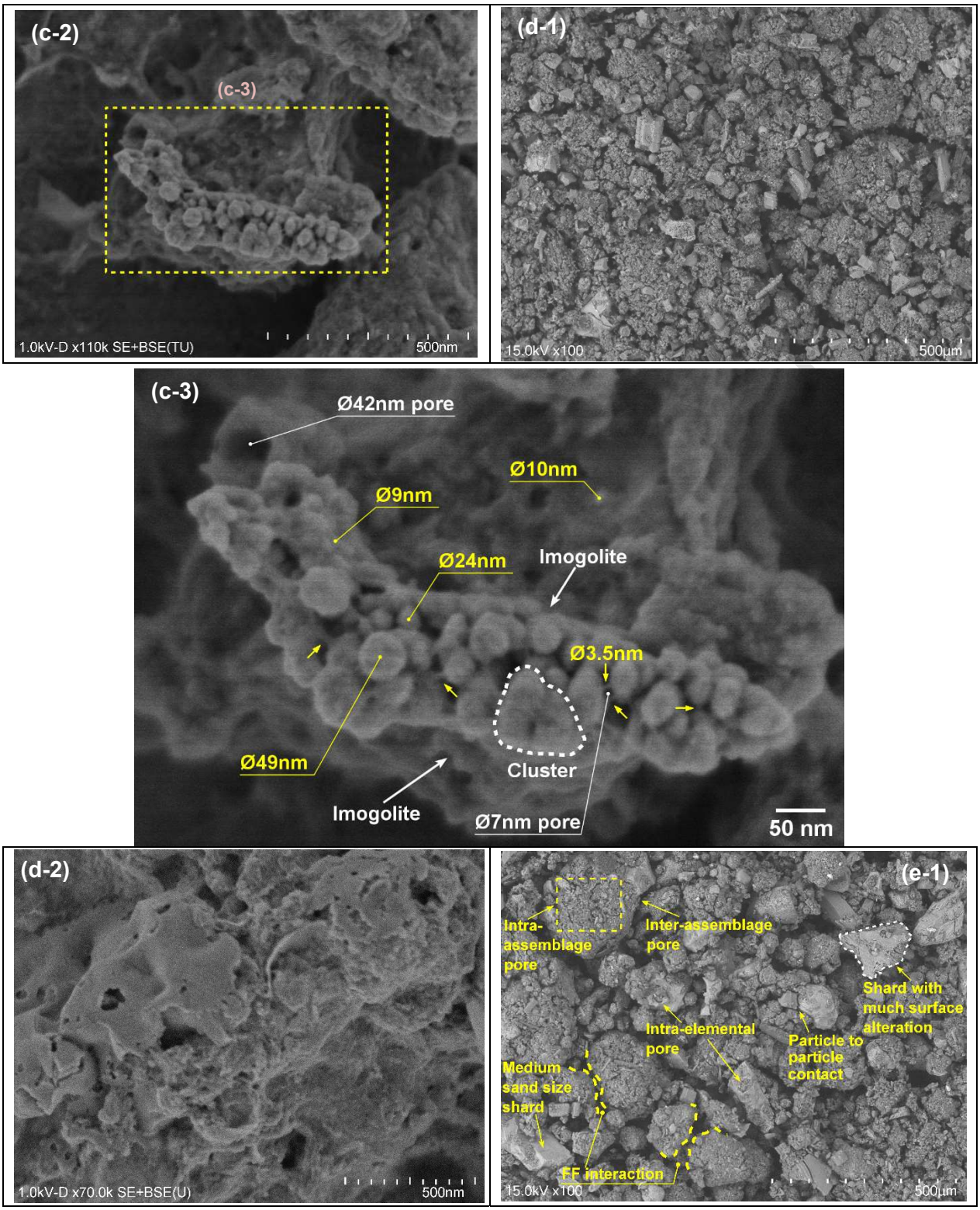

Figure 7 (c-2) FE-SEM image of Soil 1B showing arrays of allophane domains surrounded by imogolite fibres; **(c-3)** Magnified image of inset region in **(c-2)** showing allophane domains varying between 9 and 49 nm. The genesis of an allophane cluster can also be observed. The allophane domains with the imogolite fibres may display a morphology similar to an inverted micelle; **(d-1)** SEM image of Soil 1C; **(d-2)** FE-SEM image of Soil 1C showing random abrasion of imogolite fibres; **(e-1)** SEM image of Soil 2 showing the different types pores at this magnification level, face to face (FF) and particle to particle interaction

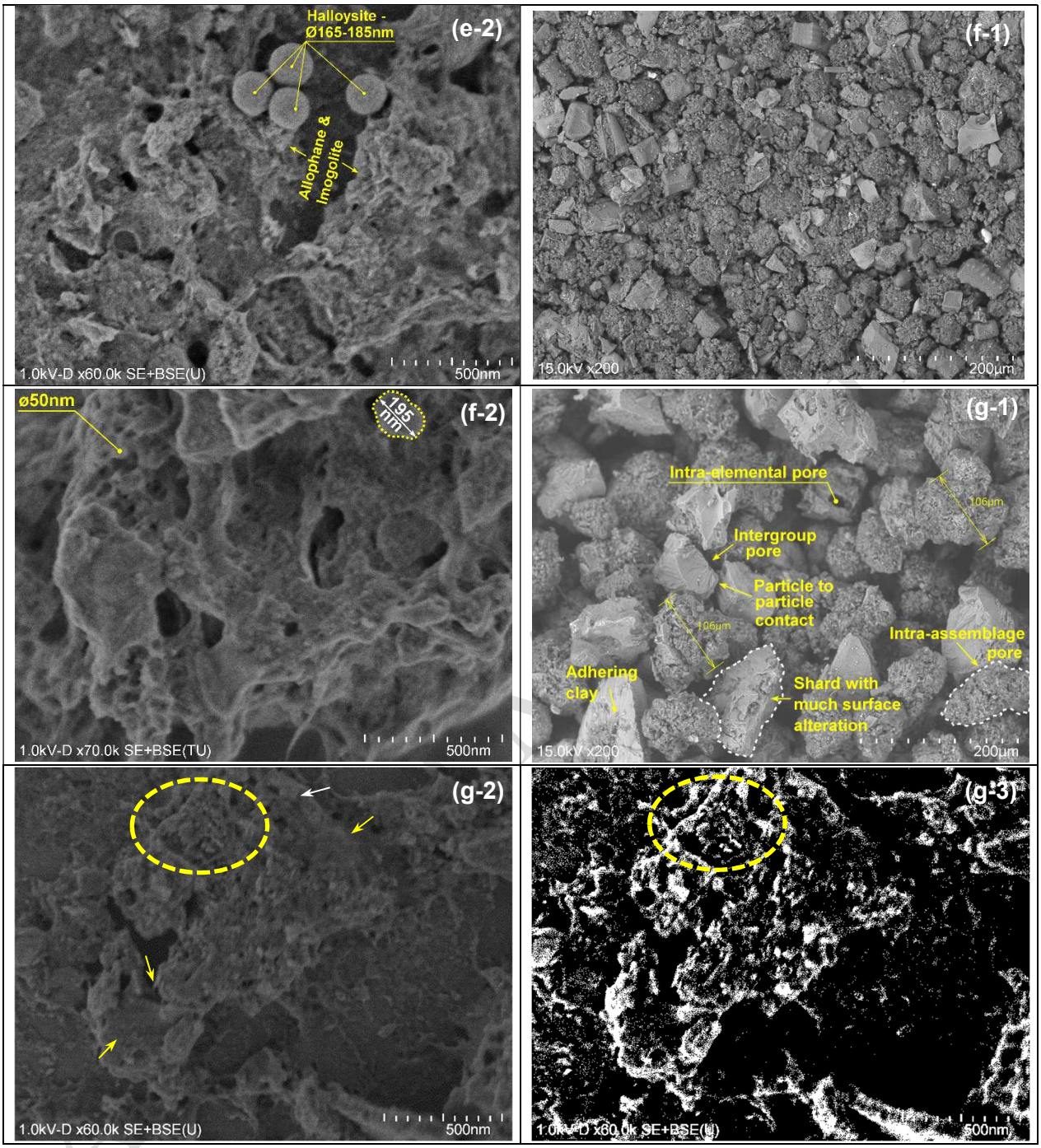

Figure 7 (e-2) FE-SEM image of Soil 2 showing presence of spherical halloysite particles together with allophane and imogolite fibres; **(f-1)** SEM image of Soil 2A; **(f-2)** FE-SEM image of Soil 2A showing a large allophane domain of 195nm; **(g-1)** SEM image of Soil 2B emphasizing the aggregation of clay particles after drying. Intra-elemental pores in volcanic shards from site 2 are clearly visible; **(g-2)** FE-SEM image of Soil 2B. Yellow arrows indicate the areas where the flaky imogolite particles are present and the dotted ellipse indicate dehydrated allophane domains. White arrow indicate occasional allophane domains marginally affected by drying; **(g-3)** Same FE-SEM image of Soil 2B as in **(g-2)** with the colours and hues adjusted to better appreciate the dehydrated allophane as observed in **(g-2)**.

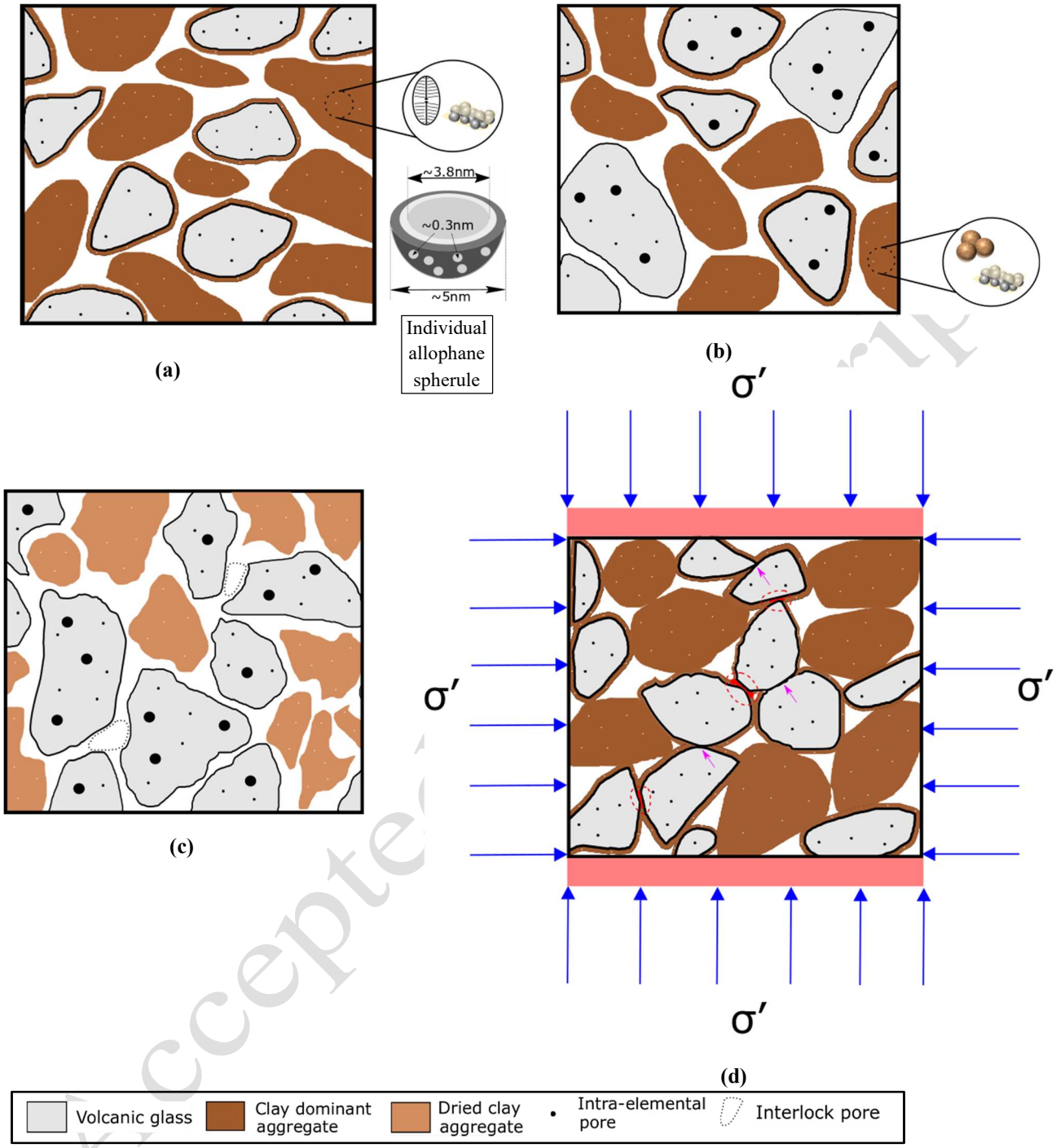

Figure 8 Conceptual microstructure model: **(a)** Soil 1 (blow-up shows presence of diatom, allophane and imogolite). White dots represent the intra-pores within the clay aggregates, while white space around the aggregates/particles are the inter-assemblage pores. Allophane spherule after Iyoda *et al.* (2012); **(b)** Soil 2 (blow-up shows presence of halloysite, allophane and imogolite); **(c)** Soil 2B with dried aggregates and interlock pores; **(d)** contact relation in Soil 1C under application of effective confining stress, σ'. Purple arrows designate grain to grain contact, red shading between grains indicate buttress type of contact and full brown contact represent face to face interaction.

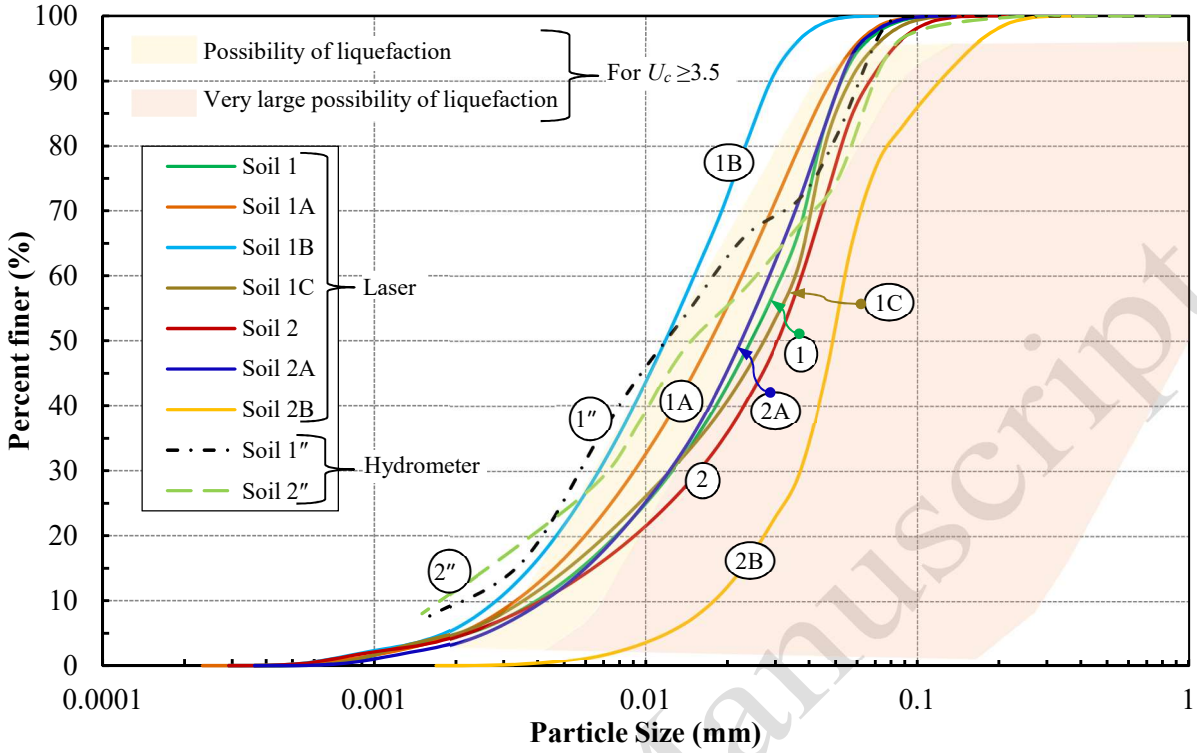

Figure 9 Grain size distribution curves of soils tested (envelopes shown from The Overseas Coastal Area Development Institute of Japan, 2009).

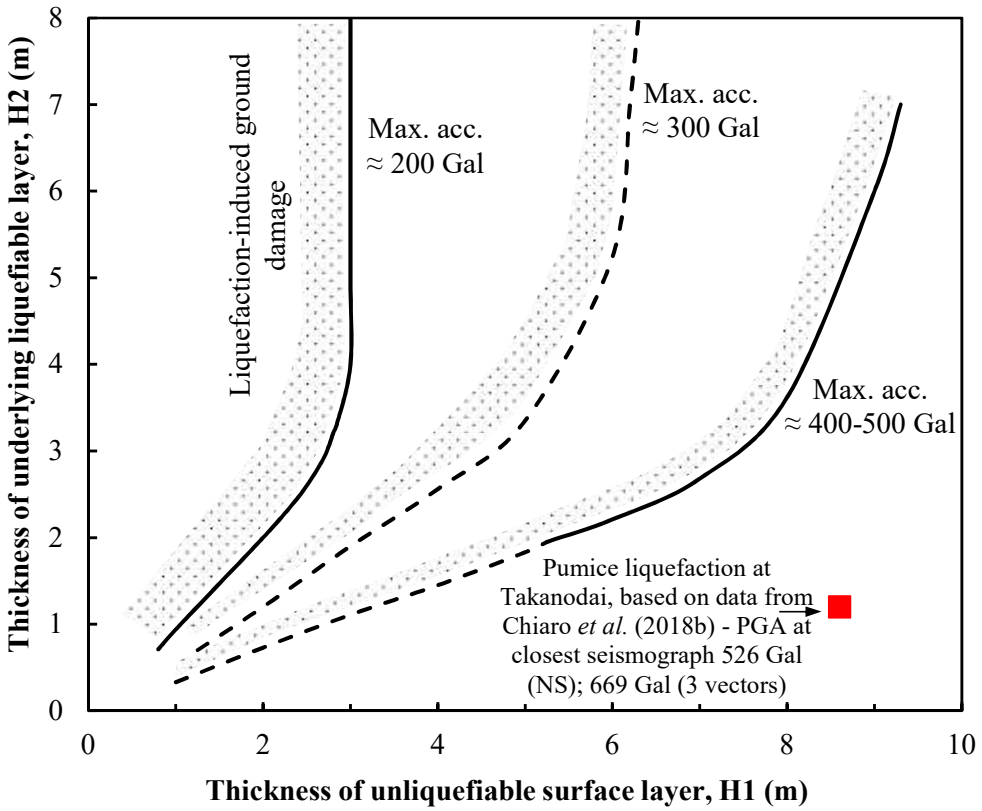

Figure 10 Proposed boundary curves for site identification of liquefaction-induced after Ishihara (1985)

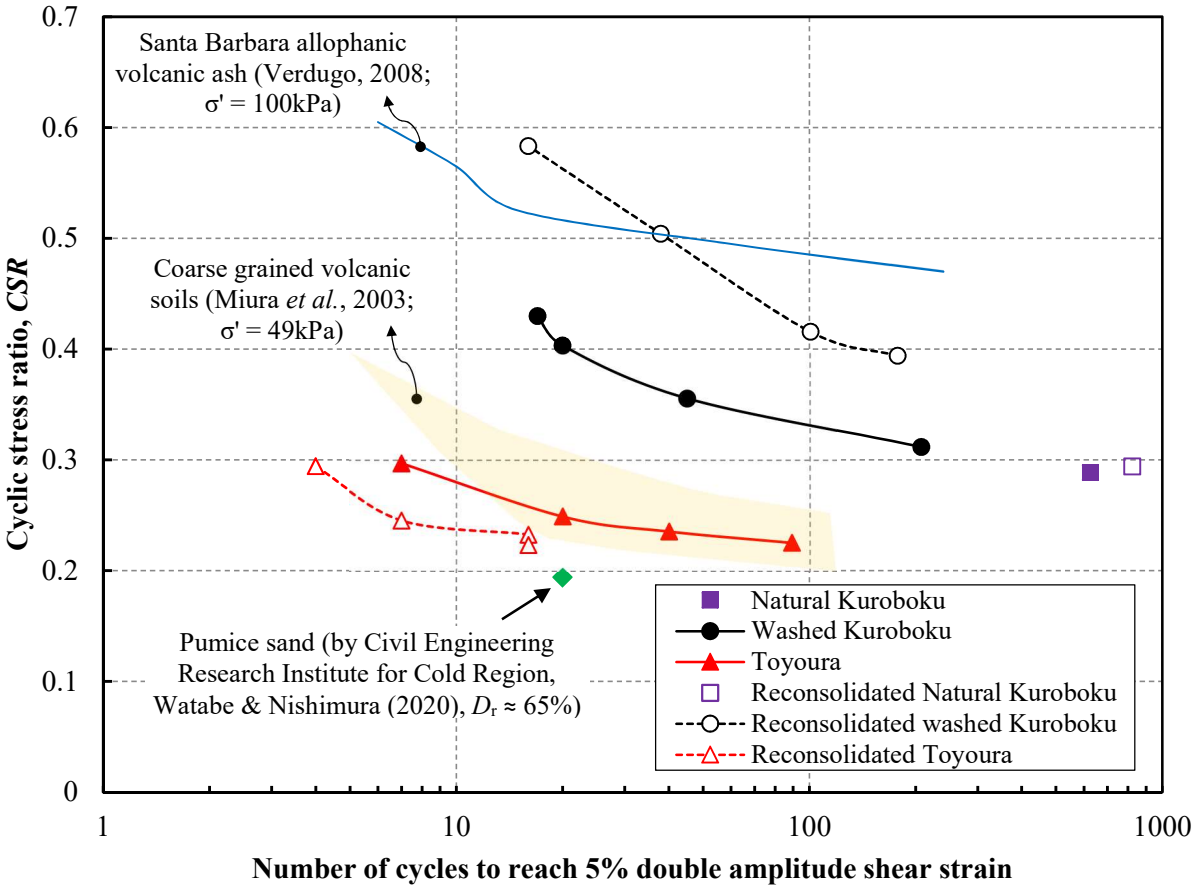

Figure 11 Cyclic strengths of natural and washed kuroboku compared with other soils (Modified with permission from Liu, 2019). Note that Verdugo (2008) and Watabe and Nishimura (2020) defined liquefaction as number of cycles to reach an excess pore water pressure ratio, R_u of 1 and 0.95 respectively.

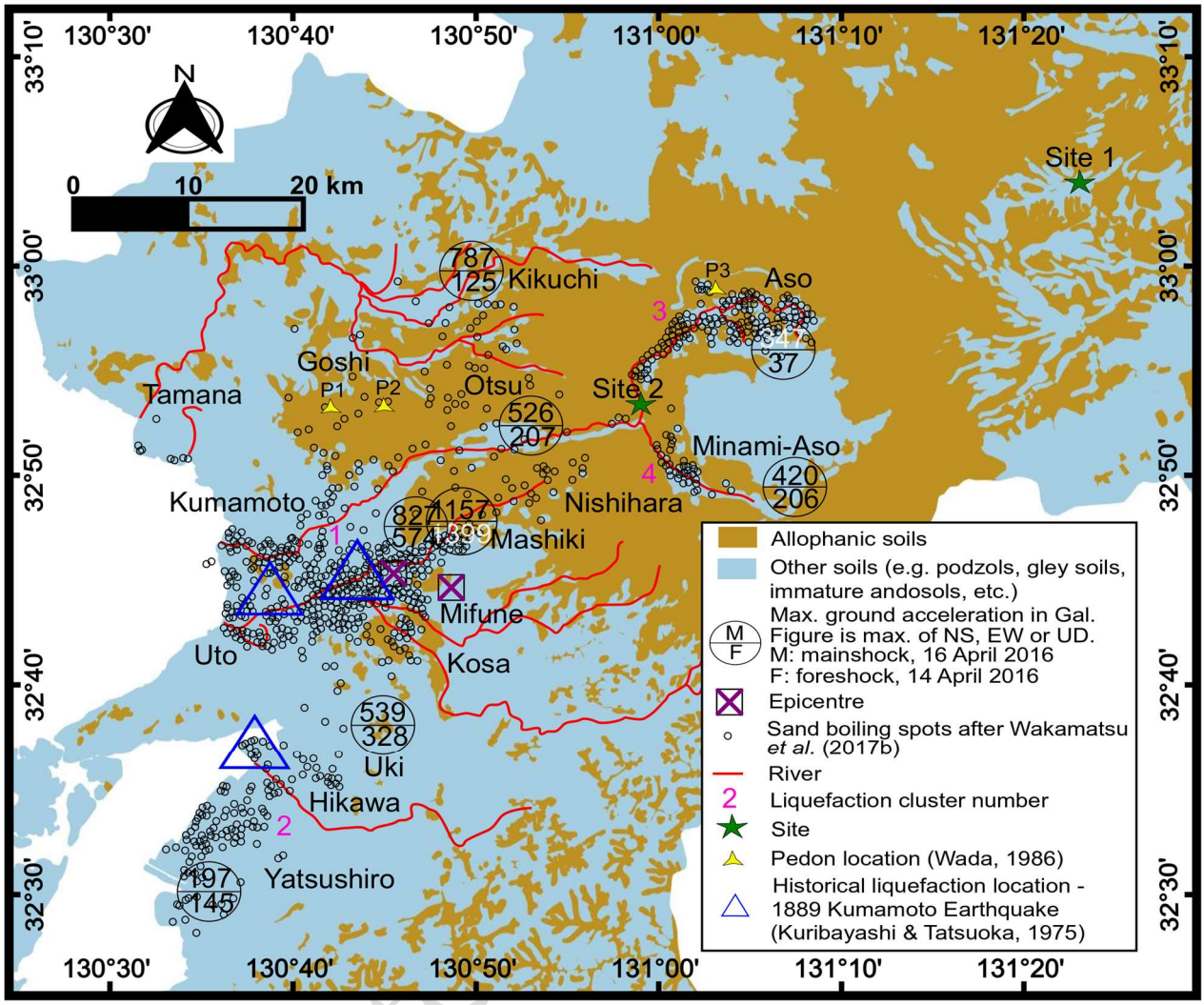

Figure 12 Soil distribution map in central Kyushu based on data from NARO (2022). Allophanic soils are represented by *brown* shading while other soils (e.g. podzols, immature andosols, gley soils) are shown in *light blue* colour. Peak Ground Acceleration - PGA (in Gal) from NIED (2022) are included at the location of the respective seismographs. The values at the *upper and bottom half of the circle* correspond respectively to the PGA of the mainshock and foreshock events of the 2016 Kumamoto earthquake. The figure displayed is the mode of PGA in NS, EW or UD direction. The sand boilings locations observed by Wakamatsu *et al.* (2017b) were superimposed on the map. The locations of pedon from Wada (1986) have also been included. Blue *triangles* represent the liquefied sites during the 1889 Kumamoto Earthquake.

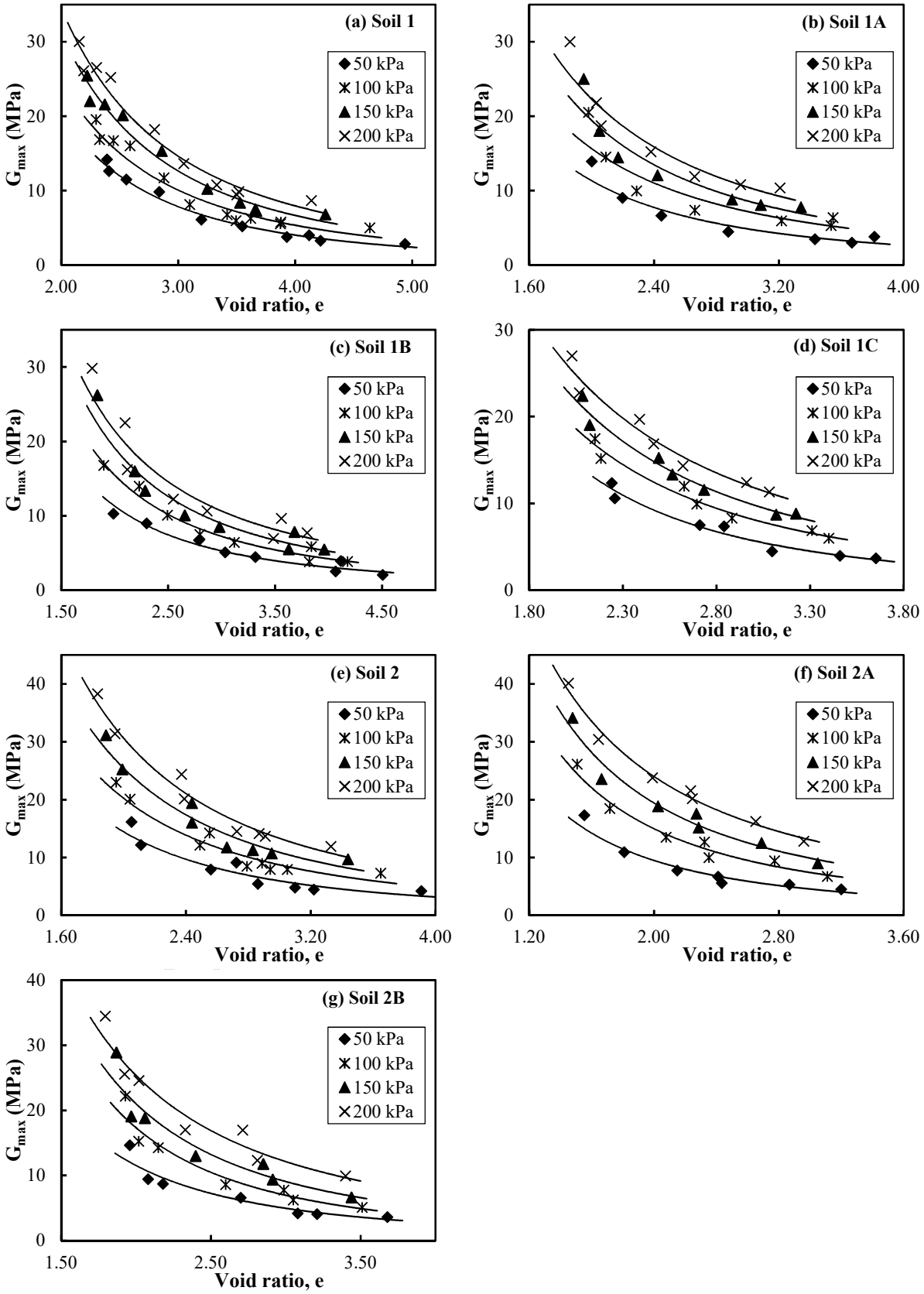

Figure 13(a-g) Variation of small- strain shear modulus (G_{max}) with void ratio

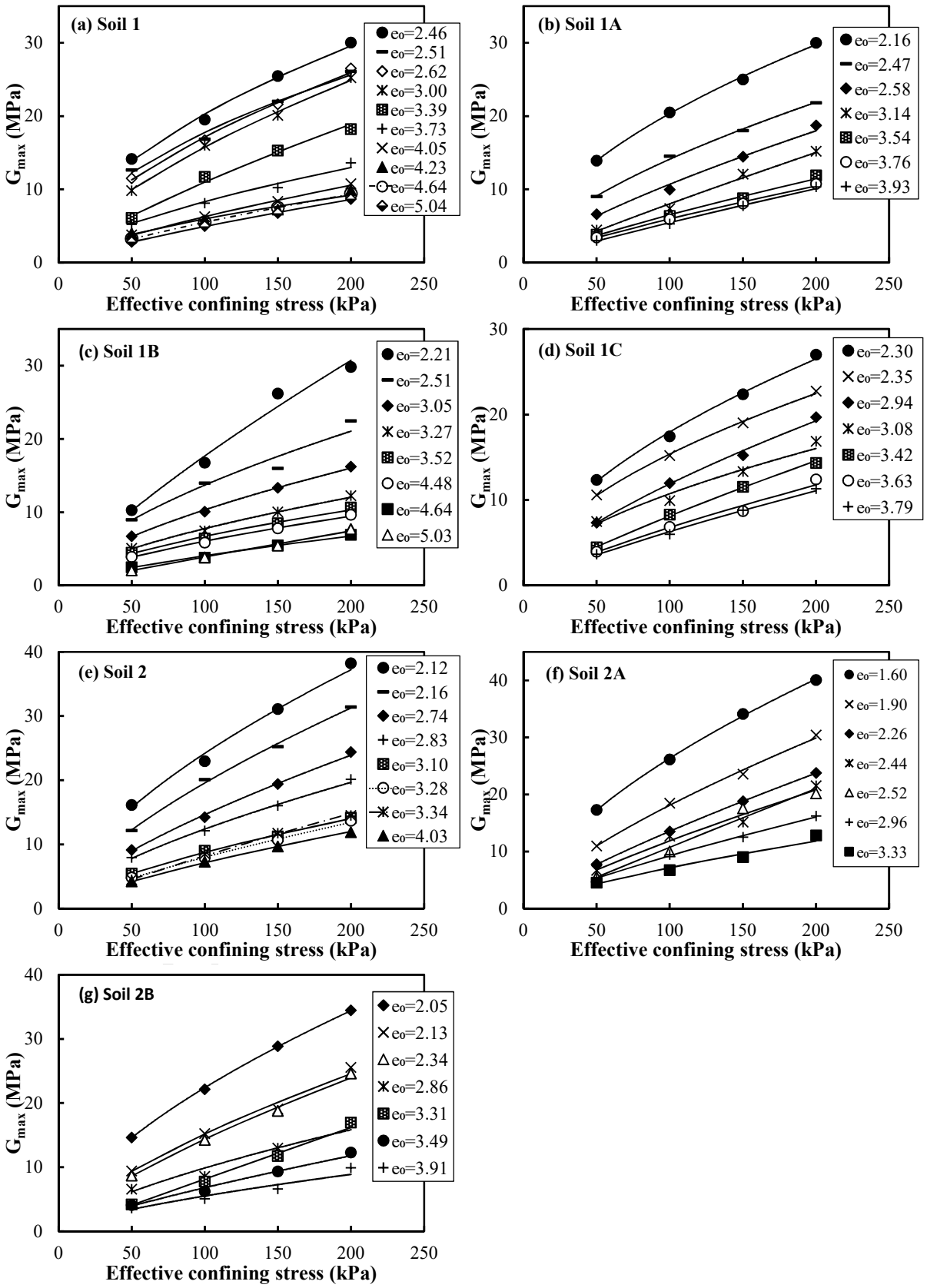

Figure 14(a-g) Variation of small- strain shear modulus (G_{max}) with effective confining stress

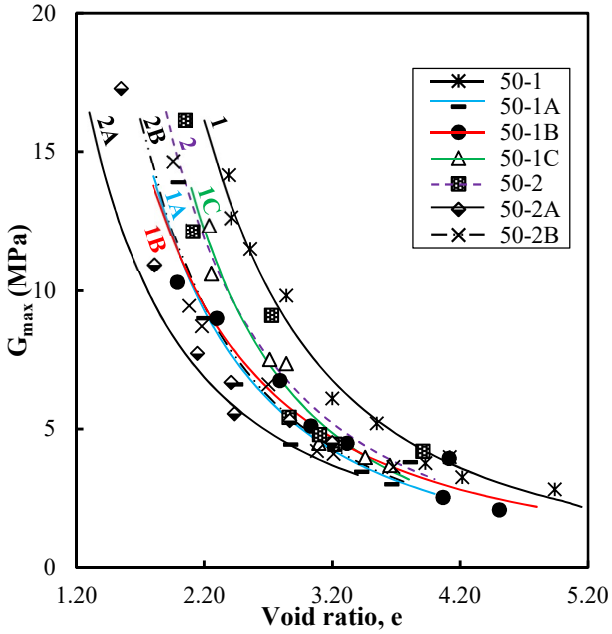

Figure 15(a) Variation of small- strain shear modulus (G_{max}) with void ratio (50kPa)

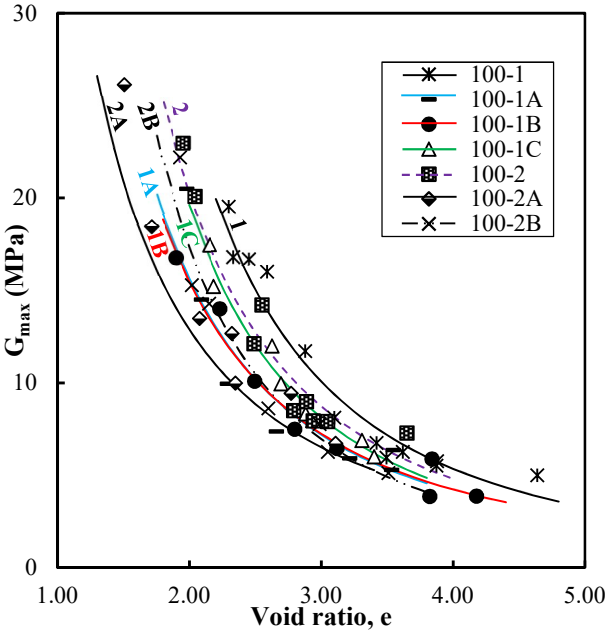

Figure 15(b) Variation of small- strain shear modulus (G_{max}) with void ratio (100kPa)

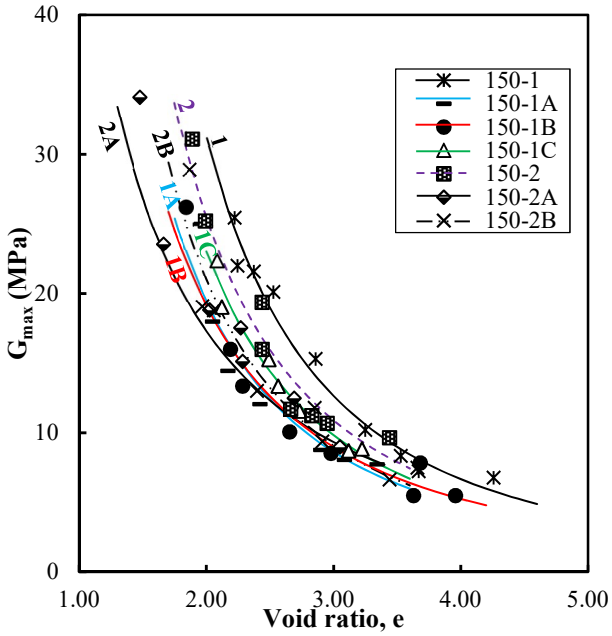

Figure 15(c) Variation of small- strain shear modulus (G_{max}) with void ratio (150kPa)

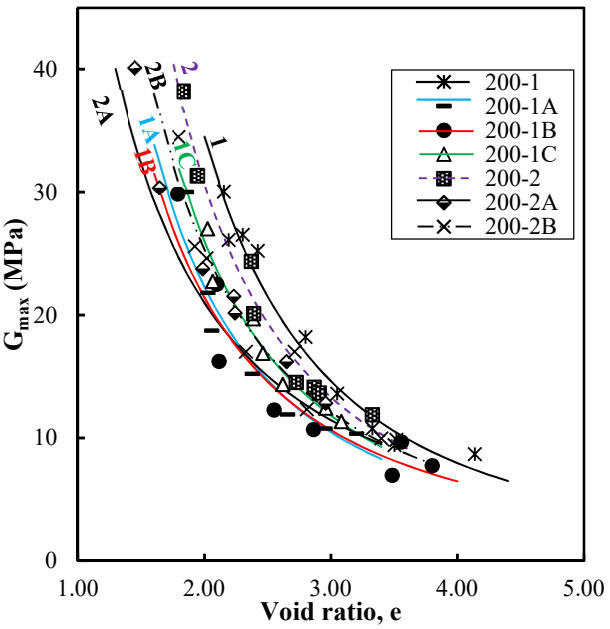

Figure 15(d) Variation of small- strain shear modulus (G_{max}) with void ratio (200kPa)

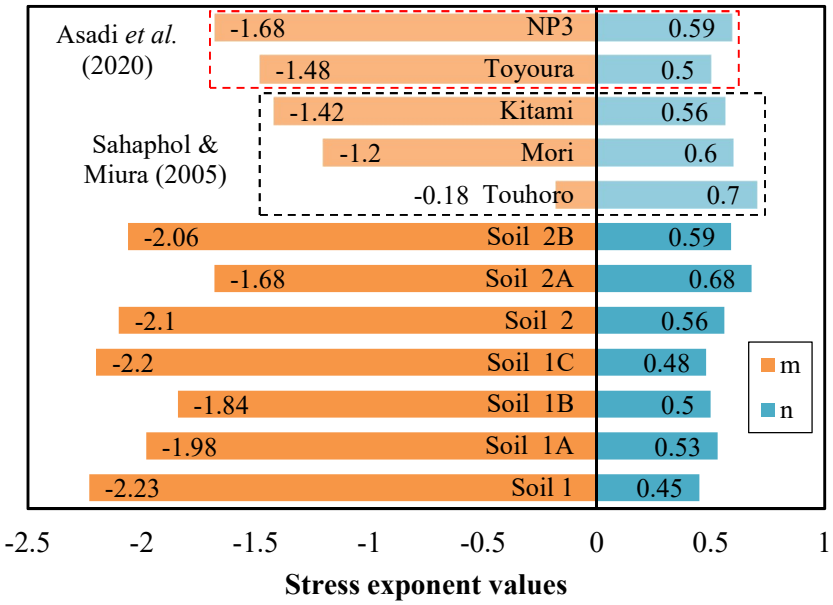

Figure 16 Comparison of stress exponents

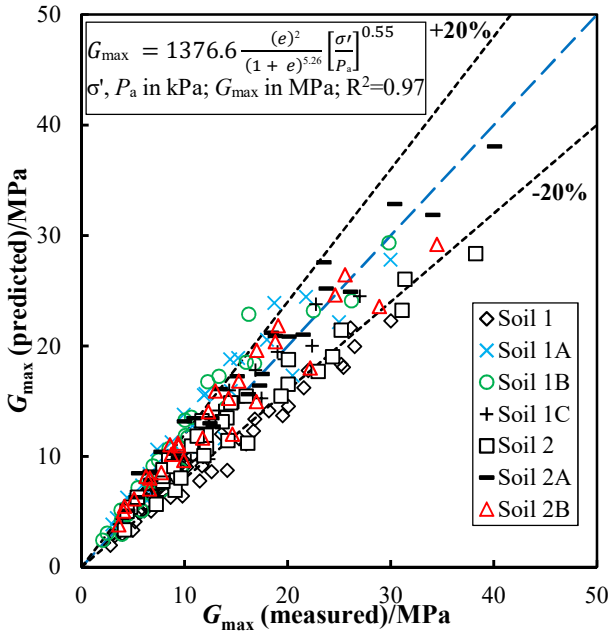

Figure 17 Predicted and measured values of small- strain shear modulus, G_{max} (Hyperbolic void ratio function)

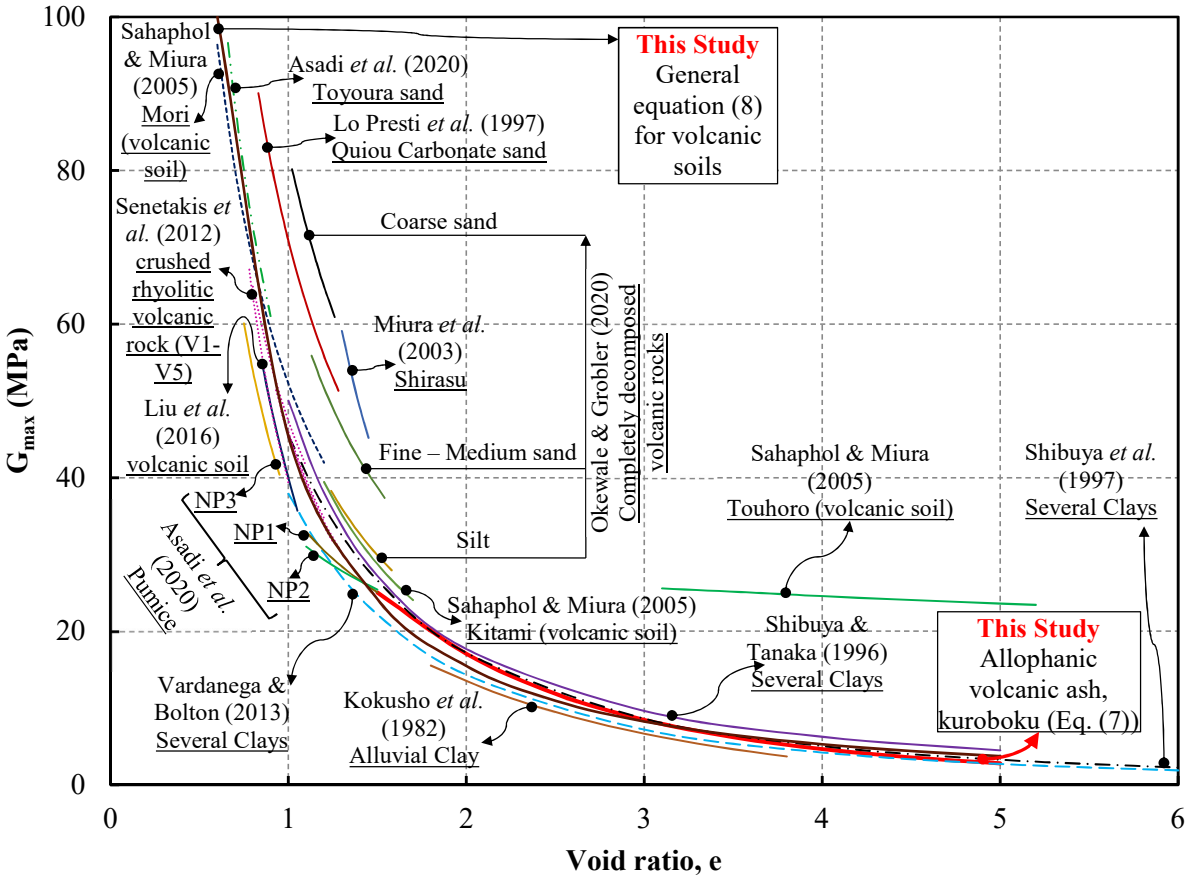

Figure 18 Variations of small- strain shear modulus (G_{max}) with void ratio for kuroboku compared with other soils (100kPa).